LA-UR-23-32645

Approved for public release; distribution is unlimited.

Title:	Role of n-phenyl-ß-naphthylamine in the Acid-Nitroplasticizer Thermal Aging (ANTA) Experiment
Author(s):	Chen, Kitmin; Kress, Joel David; Yang, Dali; Edgar, Alexander Steven; Marina, Oana C.; Li, Zhenghua; Brett, Jack Kevin
Intended for:	Report
Issued:	2023-11-06

Role of n-phenyl-β-naphthylamine in the Acid-Nitroplasticizer Thermal Aging (ANTA) Experiment

(FY2023 Annual Report for Aging and Lifetimes Program)

Kitmin Chen[a], Joel D. Kress[b], Dali Yang[a] (dyang@lanl.gov)
Alexander S. Edgar[a], O. C. Marina[c], Zhenghua Li[c], Jack K. Brett[a]

[a]MST-7: Engineered Materials, Materials Science and Technology Division
[b]T-1: Physics and Chemistry of Materials, Theoretical Division
[c]EES-14, Earth System Observations, Earth and Environmental Sciences Division,
Los Alamos National Laboratory, Los Alamos, NM 87545, United States

Abstract

A short-term aging study, which was named as Acid-Nitroplasticizer Thermal Aging (ANTA), was conducted to explore the complex chemistry between n-phenyl-β-naphthylamine (PBNA), HNO_x, and nitroplasticizer (NP). Aging of NP with PBNA and acid treatments have demonstrated that PBNA is an effective antioxidant and an anti-hydrolytic agent (e.g., inhibits HNO_3) and have allowed the identification of nitroso-PBNA (PBNA-NO). The direct conversion of PBNA to PBNA-NO via scavenging of HONO, known as nitrosation, is a preceding event of PBNA nitration, which provides evidence to the HONO elimination as the key mechanism in the early stage of NP aging. Through the kinetics of both nitrosation and nitration, the accuracy of a prediction on PBNA consumption in NP degradation is further improved.

1. Introduction

Nitroplasticizer (NP) is a binder component commonly used in energetic composites to reduce mechanical sensitivity, and consists of an approximate 1:1 (w/w) eutectic blend of bis(2,2-dinitropropyl) acetal and bis(2,2-dinitropropyl) formal (BDNPA/F) with 0.1 wt. % (6339 μM) of n-phenyl-β-naphthylamine (PBNA)[1-3]. In the past decade, our research on NP degradation has been mainly focused on the most abundant components, BDNPA/F, providing a solid ground for the nitrous acid (HONO) elimination and decomposition mechanism and the generation of water, various nitrogen oxides, and nitric acid (HNO_3)[1-5]. Recently, through the 44-month aging experiment and the use of ion chromatography (IC) and liquid chromatography quadrupole time-of-flight mass spectrometry (LC-QTOF), the role of PBNA is determined as of great importance in protecting NP from oxidation and hydrolysis despite its low concentration in NP[6, 7]. As the dominant degradants of NP, HONO, and HNO_3 can break down into $NO_2^{\bullet}$ and NO_2^+, respectively[7-12]. Scavenging of these reactive species by PBNA, also known as nitration, reduces their reactivity and acidity and thus prolongs the stability of NP. Although the nitration pathway of PBNA has been firmly identified, some critical details on the early stage of NP degradation are missing as the PBNA concentration detected in the unaged NP is considerably low (757 μM) and an intimate association is found between PBNA and an unknown compound at m/z 219.1047[6]. Additionally, direct evidence of PBNA in the reduction of acidity is needed to attest to its

application in prolonging the shelf-life of NP. The chemistry of HONO and HNO_3 reactions is extremely complex because of the different HNO_x (x = 1, 2, 3), NO_y (y = 1, 2) and N_2O_z (z = 1, 2, 3, 4, 5) species involved, which are given by a series of papers: (1) the ionic equilibrium of the thermal decomposition of HNO_3 in the liquid phase by Robertson et al.[8]; (2) the self-ionization mechanism as one of the physicochemical properties in concentrated HNO_3 described by Stern et al.[9] and further reiterated in Ziouane and Leturcq's dissociation model of HNO_3 as a function of acidity and temperature[10]; (3) the decomposition of HNO_3 to nitrogen oxides and water in supercritical water by Chlistunoff et al.[11]; (4) the mechanism of heterogeneous NO_2 hydrolysis between gas phase and water film by Wingen et al.[12]; and (5) the theoretical-based reaction network by Bruggemann et al., which covers the various reaction pathways among the nitrogen oxides prior to reacting with ammonia in a zeolite-catalyzed environment[13]. Therefore, a 21-week short aging experiment, called Acid-Nitroplasticizer Thermal Aging (ANTA), was judiciously designed and conducted, which isolates the interaction between PBNA and HNO_x and explores the chemistry occurring in the early stage of NP degradation. The detection of nitrosation has shed new light on the role of PBNA how this antioxidant scavenges HONO directly, which has never been reported previously. Through these studies, PBNA is proven as an effective antioxidant, as well as an anti-hydrolytic agent for NP.

2. Experimental

2.1 Sources of NP

Although the NP used for the ANTA experiment has the same lot number (OCP-A/F-XB 8/8, drum #1, made around 1965), suggesting that it came from the same source as the NP used in the 44-month aging experiment, the former NP was obtained from TA-9 laboratory on 07/2012[14]. This NP has been stored in TA-9 laboratory where the temperature largely changed with seasonal temperatures. Its container had been routinely opened when needed for various usages. As expected, the headspace of its container increased as more NP had been consumed and accordingly the headspace composition had been constantly altered upon each opening. On the other hand, the NP used in the 44-month aging experiment was obtained from a tightly sealed container on 02/2016, which was stored inside a cold place at another location in TA-9. To differentiate two NP sources, the NP obtained from the tightly sealed container is called inert NP.

2.2 ANTA Approach

Compared to the PBNA concentration in the inert NP (757 μM), the lower PBNA concentration in the TA-09 NP (81 μM) is expected and likely the result of frequent disturbance of volatile equilibrium in the container headspace. Based on the previous studies[2, 5-7, 15, 16], the elevated thermal effect of 64°C caused complex and unpredictable reactions that greatly deviate from the normal NP degradation rate. Therefore, in this study, the aging temperatures were selected at 25, 35, 45 and 55°C. The ANTA experiment consists of 8 treatment types, as described in Table 1. While C, P, PH, H1, H2, H3, and H4 were aged for 3, 6, 10, 17, and 21 weeks (5 periods), H5 is identical to H4 but accidentally heated at an unknown temperature for less than 30 min (i.e., condensation was observed) due to the incorrect stirrer being used, as shown in Figure 1. Instead

of disposing the H5 samples, they were also aged at 35, 45, and 55°C (excluded 25°C) and monitored at earlier weeks (1, 2, 4, 5, 7, and 9 weeks) for any significant changes, which the results are later confirmed similar to the H4 samples. Therefore, a total of 31 sets (i.e., 8 types × 4 temperatures – H5 at 25°C = 31 unique experimental conditions), which yield a total of 158 NP samples prepared, as depicted in Table 1 and shown in Figure 2.

Table 1. ANTA study sample sets and sample counts.

Set Index	Treatment type	Sample quantity per temperature				Sample total per type
		25°C	35°C	45°C	55°C	
C	Control, no reagents added	5	5	5	5	20
P	0.1% PBNA	5	5	5	5	20
PH	0.1% PBNA and 1400 µM HNO_3	5	5	5	5	20
H1	350 µM HNO_3	5	5	5	5	20
H2	700 µM HNO_3	5	5	5	5	20
H3	1050 µM HNO_3	5	5	5	5	20
H4	1400 µM HNO_3	5	5	5	5	20
H5	1400 µM HNO_3, heated	N/A	6	6	6	18
		Total number of samples prepared				**158**

C = control, P = PBNA addition, and H = HNO_3 addition

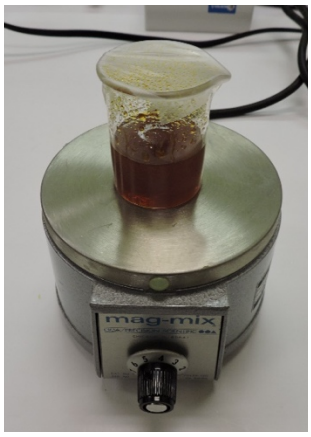

Figure 1. H5 was accidentally heated on the stirrer, resulting in some condensation.

Figure 2. A total of 158 ANTA samples. (Not all samples are shown in the picture.)

2.3 Aging Sample Preparation

All glassware and magnet bars were cleaned with LCMS grade water and acetonitrile (ACN) to eliminate impurities. To ensure the starting NP materials are the same across all samples, five 40-mL glass vials and one 20-mL vial of TA-9 NP were combined and stirred in a 600-mL beaker (sealed with parafilm) for more than 1 hour. From the combined total of approximately 200 mL (278 g, density 1.39 g/mL) of homogenized TA-9 NP, 30.6 g were weighed in a 50-mL beaker for each treatment type, as shown in Figure 3. As summarized in Table 2, the weighed NP samples were treated with various amount and types of reagents, including PBNA (Sigma, SKU: 178055, 97% Purity), HNO_3 (Sigma, ACS grade, 70%), and LCMS grade water (Fisher Chemical, Optima).

Before storing in refrigerator (< 8°C), parafilm was used in covering all beakers to avoid excessive exposure to air and to minimize volatile losses during the weighing process, as shown in Figure 4.

Figure 3. Five vials of 40-mL and one vial of 20-mL TA-9 NP (left) are combined in a 600-mL beaker and distributed to the 50-mL beakers (right). The correct NP lot number is OCP-A/F-XB 8/8 rather than X-B 48/8 as shown on the vial labels.

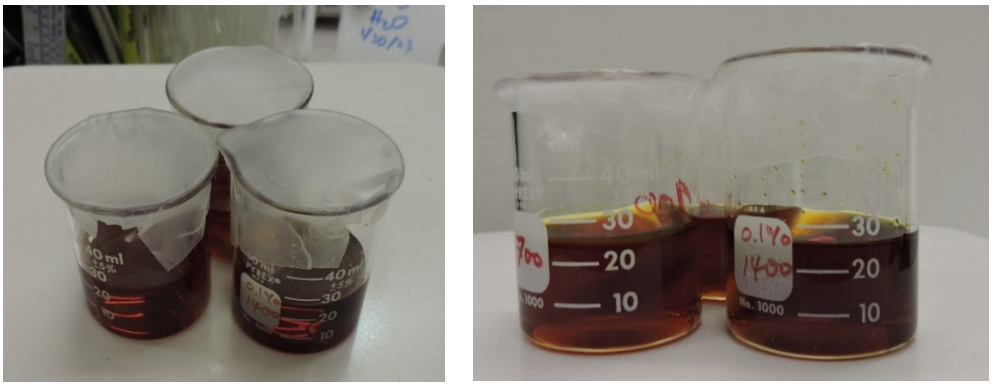

Figure 4. Treated NP samples are covered with parafilm to minimize air exposure.

Table 2. Addition of reagents and their expected concentrations in the treated NP samples.

Sample type	NP weight (g)	PBNA add. (g)	Water add. (µL)	1M HNO_3 add. (µL)	Calc. PBNA (%)	Calc. HNO_3 Conc. (µM)	Calc. water total vol. (µL)	Calc. water conc. (ppm)
C	N/A	N/A	N/A	N/A	N/A	N/A	N/A	N/A
P	30.58625	0.03053	29.4	N/A	0.0998	N/A	N/A	N/A
PH	30.58545	0.03033	N/A	30.8	0.0992	1399.75	29.41140	961.61416
H1	30.58102	N/A	22.1	7.7	N/A	349.99	29.45285	963.10883
H2	30.59218	N/A	14.7	15.4	N/A	699.72	29.41570	961.54314
H3	30.58089	N/A	7.4	23.1	N/A	1049.97	29.43855	962.64534
H4	30.59058	N/A	N/A	30.8	N/A	1399.52	29.41140	961.45290
H5	30.58767	N/A	N/A	30.8	N/A	1399.65	29.41140	961.54436

2.3.1 PBNA addition and Homogeneity

To demonstrate dissolution and homogenization of PBNA in the NP samples can be achieved by a stirring method, a test trial of 25.343 g of NP mixed with 29.6 mg of PBNA (i.e., equivalent to an expected 0.1168 wt.% PBNA in NP) was prepared by stirring on a magnetic stirrer for 30 min. Five different regions of the mixture were sampled and analyzed by LC-QTOF, including peripheral-top (PT), peripheral-mid (PM), peripheral-bottom (PB), center-top (CT), and center-mid (CM), as illustrated in Figure 5. Based on the coefficient of variation (CV = std. dev./mean)

of less than 17% between different sampling regions across all targeted analytes (e.g., mononitro-PBNA, dinitro-PBNA, BDNPA, BDNPF and PBNA), as presented in Table 3, the mixture of NP and PBNA is confirm homogenized. This tester NP was not used in further experiment because the origin of this NP is not known.

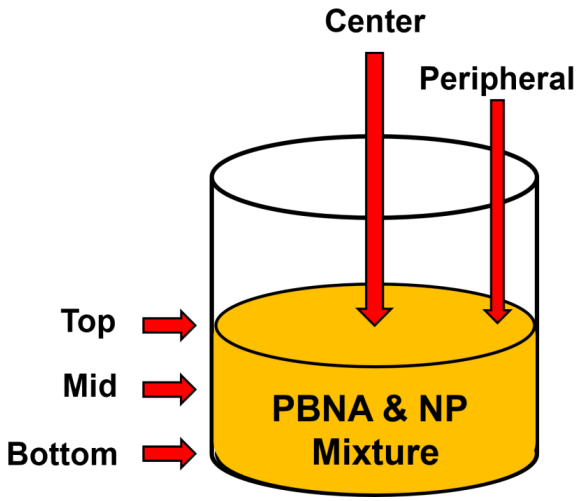

Figure 5. Sampling regions of PBNA & NP mixture for homogeneity.

Table 3. Statistical evaluation of 3-mg samples from five sampling regions (PT, PM, PB, CT, CM).

Sample weight	Statistic of PT, PM, PB, CT, and CM	mononitro isomer 1	mononitro isomer 2	mononitro isomer 3	dinitro isomer 1	dinitro isomer 2	BDNPA	BDNPF	PBNA
3 mg	STDEV (cps^2)	57886	98039	36461	87769	78115	1212269	292967	3340730
	MEAN (cps^2)	356340	581296	214052	616601	487460	12111089	4072302	22560040
	CV (%)	16.2	16.9	17.0	14.2	16.0	10.0	7.2	14.8

STDEV = standard deviation; CV = coefficient of variability
3 mg NP sample dissolved in 10 mL ACN for LC-QTOF analysis[6, 15]

To verify the accuracy of sampling representation, the sampling weight was increased to 50 mg from 3 mg to prepare samples from the top, mid, and bottom of the center region. Compared to 3 mg[6, 15] , 50 mg is significantly lower in variability (< 8%), as shown in Table 4. The reduced intensity in the 50-mg samples is due to a lower injection volume (3 µL instead of 5 µL). Therefore, the sampling weight of 50 mg is adopted for latter LC-QTOF sample preparation. Provided by the five repeated injections of each 50-mg samples, the repeatability of instrumental responses is also substantiated at less than 8%. Based on the LC-QTOF results from different regions, the accuracy of the added PBNA amount in the test trial is determined at 80.3 ± 13.1%.

Table 4. Statistical evaluation of 50-mg samples (top, mid, bottom).

Sample weight	Statistic of top, mid, and bot.	mononitro isomer 1	mononitro isomer 2	mononitro isomer 3	dinitro isomer 1	dinitro isomer 2	BDNPA	BDNPF	PBNA
50 mg	STDEV (cps^2)	11650	22370	9710	23634	20490	489606	146374	998091
	MEAN (cps^2)	220005	338875	127660	376400	282367	9236942	2947018	13897653
	CV (%)	5.3	6.6	7.6	6.3	7.3	5.3	5.0	7.2
	Instrumental Repeatability	5.7	5.9	7.6	6.3	7.2	5.1	5.2	7.4

50 mg NP sample dissolved in 10 mL ACN and diluted 10-fold (100 µL aliquot + 900 µL ACN) for LC-QTOF analysis

2.3.2 HNO_3 Addition

To avoid aggressive reaction between NP and concentrated HNO_3 and to allow the use of the digital pipettes for the addition of HNO_3, a 1 M working solution of HNO_3 was prepared by diluting 0.45503 g of the concentrated HNO_3 (70% or 15.7M, density = 1.413 g/mL) in a 5-mL volumetric flask with LCMS grade water, which yield 4.51% HNO_3 in water, as calculated in Eq. (1). Based on the aliquot volume of added 1 M HNO_3 and the NP (density 1.39 g/mL) sample weight per addition type, the expected HNO_3 concentrations are calculated, as exemplified using H2 in Eq. (2).

$$\frac{mass\ of\ conc.\ HNO_3}{density\ of\ conc.\ HNO_3} \times \frac{conc.\ of\ HNO_3}{final\ volume} = \frac{0.45503\ g\ conc.\ HNO_3}{1.413\ g/mL} \times \frac{15.7\ M\ or\ 70\%}{5\ mL} = 1.01\ M\ or\ 4.51\%\ HNO_3 \quad \textbf{Eq. (1)}$$

$$[HNO_3]\ in\ H2 = \frac{aliquot\ volume\ \times 1\ M\ HNO_3}{\frac{mass\ of\ NP\ sample}{density\ of\ NP} \times unit\ conversion} = \frac{30.8\ \mu L \times 1\ M}{\left(\frac{30.59058\ g\ NP}{1.39\ g/mL} \times \frac{1\ mL}{1000\ \mu L}\right)} = 1399.52\ \mu M \quad \textbf{Eq. (2)}$$

2.3.3 Water Addition

Since the HNO_3 concentration, temperature, and aging time are the primary manipulating variables of the ANTA experiment, other control variables such as water must be maintained at a constant concentration. Because a 1 M HNO_3 solution consists of 95.54% water, aliquots of water (in µL) were added to account for the discrepancy of water concentrations in between different acid additions. The expected total water volumes and concentrations in the NP samples are calculated, using H2 as an example, as shown in Eq. (3) and Eq. (4), respectively.

$$Total\ H_2O\ vol.\ in\ H2\ sample = \%H_2O\ in\ 1\ M\ HNO_3\ \times aliquot\ vol.\ of\ HNO_3 + \ aliquot\ vol.\ of\ H_2O$$

$$= 0.9554\ \times\ 15.4\ \mu L\ +\ 7.7\ \mu L = 29.41570\ \mu L \quad \textbf{Eq. (3)}$$

$$[H_2O]\ in\ H2 = \frac{Total\ H_2O\ vol.\ \times unit\ conversion}{mass\ of\ NP} = \frac{29.41570\ \mu L \times \frac{1\ mL}{1000\ \mu L} \times 1\ \frac{g}{mL} \times \frac{10^6\ \mu g}{1\ g}}{30.59218\ g\ NP} = 961.54314\ ppm\ or\ \mu g/g \quad \textbf{Eq. (4)}$$

The expected concentration of 961 ppm is within the range of 572 to 2910 ppm of produced water in the aged NP samples[5], which is presented in Table 5. This small amount of water can potentially help stabilize the added HNO_3 though it may also induce minor hydrolysis of NP.

Table 5. Water concentrations of aged NP samples which NP hydrolysis is observed.

Sample Name	Water Conc. (ppm)	Sample Name	Water Conc. (ppm)	Sample Name	Water Conc. (ppm)
5A-33	1056	**6A-18**	573	**3W-12**	2910
5A-36	1042	**6A-21**	1063	**4W-02**	2105
5A-44	936	**6A-24**	1509	**5W-02**	2085

2.3.4 Weighing of ANTA samples

Weighing of the ANTA samples was completed within 2 days. In between pauses of weighing, samples were stored in the refrigerator and re-stirred at room temperature for at least 30 min to ensure homogeneity. Each 1.5-mL autosampler vial (Thermo Scientific, high recovery clear glass vial with 30 µL reservoir) contains approximately 1 mL of NP sample and is sealed with Teflon tape on the screw thread and capped with PTFE cap. In this way, exposure to air is minimized. All

samples were placed in the corresponding aging oven on the third day. Each sample is labelled in codes corresponding to their aging conditions: temperature – treatment type – aging weeks. For example, the "2H1-06" label means 1-mL of NP sample with the addition of 350 μM HNO_3 ages at 25°C for 6 weeks. The weights of all samples and their calculated volume (via default NP density of 1.39 g/mL) are listed in Table 6 to Table 13. Given by the standard deviation of less than 6.5 mg or 0.005 mL, the weighing was conducted at high precision.

Table 6. Weights of C samples

Unit label	Unit weight (mg)	Calc. Volume (mL)
2C-03	1396.94	1.0050
2C-06	1387.42	0.9981
2C-10	1388.21	0.9987
2C-15	1394.58	1.0033
2C-21	1389.17	0.9994
3C-03	1395.09	1.0037
3C-06	1392.31	1.0017
3C-10	1389.72	0.9998
3C-15	1388.69	0.9991
3C-21	1398.48	1.0061
4C-03	1390.35	1.0003
4C-06	1388.44	0.9989
4C-10	1383.09	0.9950
4C-15	1381.76	0.9941
4C-21	1391.63	1.0012
5C-03	1382.44	0.9946
5C-06	1383.18	0.9951
5C-10	1388.50	0.9989
5C-15	1382.80	0.9948
5C-21	1397.30	1.0053
STDEV	5.19	0.0037

Table 7. Weights P samples

Unit label	Unit weight (mg)	Calc. Volume (mL)
2P-03	1394.34	1.0031
2P-06	1387.38	0.9981
2P-10	1394.77	1.0034
2P-15	1388.89	0.9992
2P-21	1387.2	0.9980
3P-03	1383.13	0.9951
3P-06	1390.53	1.0004
3P-10	1398.99	1.0065
3P-15	1391.12	1.0008
3P-21	1386.66	0.9976
4P-03	1387.37	0.9981
4P-06	1396.16	1.0044
4P-10	1392.91	1.0021
4P-15	1387.31	0.9981
4P-21	1382.45	0.9946
5P-03	1388.66	0.9990
5P-06	1382.34	0.9945
5P-10	1392.09	1.0015
5P-15	1382.87	0.9949
5P-21	1387.17	0.9980
STDEV	4.72	0.0034

Table 8. Weights of PH samples

Unit label	Unit weight (mg)	Calc. Volume (mL)
2PH-03	1389.79	0.9998
2PH-06	1386.66	0.9976
2PH-10	1380.89	0.9934
2PH-15	1383.13	0.9951
2PH-21	1388.38	0.9988
3PH-03	1399.4	1.0068
3PH-06	1387.97	0.9985
3PH-10	1390.45	1.0003
3PH-15	1382.71	0.9948
3PH-21	1387.32	0.9981
4PH-03	1385.31	0.9966
4PH-06	1394.46	1.0032
4PH-10	1384.48	0.9960
4PH-15	1383.17	0.9951
4PH-21	1386.53	0.9975
5PH-03	1383.12	0.9951
5PH-06	1397.16	1.0052
5PH-10	1386.98	0.9978
5PH-15	1383.89	0.9956
5PH-21	1385.49	0.9968
STDEV	4.89	0.0035

Table 9. Weights of H1 Samples

Unit label	Unit weight (mg)	Calc. Volume (mL)
2H1-03	1396.42	1.0046
2H1-06	1387.75	0.9984
2H1-10	1386.59	0.9975
2H1-15	1392.55	1.0018
2H1-21	1389.06	0.9993
3H1-03	1389.45	0.9996
3H1-06	1392.07	1.0015
3H1-10	1383.19	0.9951
3H1-15	1386.92	0.9978
3H1-21	1395.21	1.0037
4H1-03	1388.52	0.9989
4H1-06	1383.28	0.9952
4H1-10	1388.81	0.9991
4H1-15	1386.15	0.9972
4H1-21	1385.96	0.9971
5H1-03	1395.59	1.0040
5H1-06	1386.98	0.9978
5H1-10	1395.23	1.0038
5H1-15	1394.59	1.0033
5H1-21	1390.68	1.0005
STDEV	4.11	0.0030

Table 10. Weights of H2 samples

Unit label	Unit weight (mg)	Calc. Volume (mL)
2H2-03	1384.23	0.9958
2H2-06	1394.15	1.0030
2H2-10	1384.93	0.9964
2H2-15	1382.78	0.9948
2H2-21	1393.78	1.0027
3H2-03	1399.56	1.0069
3H2-06	1393.28	1.0024
3H2-10	1397.05	1.0051
3H2-15	1396.14	1.0044
3H2-21	1398.84	1.0064
4H2-03	1389.16	0.9994
4H2-06	1382.58	0.9947
4H2-10	1386.58	0.9975
4H2-15	1398.76	1.0063
4H2-21	1385.11	0.9965
5H2-03	1392.81	1.0020
5H2-06	1382.94	0.9949
5H2-10	1398.69	1.0063
5H2-15	1393.21	1.0023
5H2-21	1388.18	0.9987
STDEV	6.07	0.0044

Table 11. Weights of H3 samples

Unit label	Unit weight (mg)	Calc. Volume (mL)
2H3-03	1394.39	1.0032
2H3-06	1398.85	1.0064
2H3-10	1387.84	0.9984
2H3-15	1398.14	1.0059
2H3-21	1393.60	1.0026
3H3-03	1391.64	1.0012
3H3-06	1380.67	0.9933
3H3-10	1384.15	0.9958
3H3-15	1385.85	0.9970
3H3-21	1396.97	1.0050
4H3-03	1381.73	0.9941
4H3-06	1388.90	0.9992
4H3-10	1385.80	0.9970
4H3-15	1384.16	0.9958
4H3-21	1392.62	1.0019
5H3-03	1385.82	0.9970
5H3-06	1399.42	1.0068
5H3-10	1384.26	0.9959
5H3-15	1399.55	1.0069
5H3-21	1392.96	1.0021
STDEV	6.22	0.0045

Table 12. Weights of H4 samples

Unit label	Unit weight (mg)	Calc. Volume (mL)
2H4-03	1383.27	0.9952
2H4-06	1385.65	0.9969
2H4-10	1390.92	1.0007
2H4-15	1394.43	1.0032
2H4-21	1385.32	0.9966
3H4-03	1391.48	1.0011
3H4-06	1393.08	1.0022
3H4-10	1380.72	0.9933
3H4-15	1393.79	1.0027
3H4-21	1386.38	0.9974
4H4-03	1390.95	1.0007
4H4-06	1383.37	0.9952
4H4-10	1385.69	0.9969
4H4-15	1383.35	0.9952
4H4-21	1394.14	1.0030
5H4-03	1384.57	0.9961
5H4-06	1386.14	0.9972
5H4-10	1394.32	1.0031
5H4-15	1393.73	1.0027
5H4-21	1385.07	0.9965
STDEV	4.60	0.0033

Table 13. Weights H5 samples

Unit label	Unit weight (mg)	Calc. Volume (mL)
3H5-01	1394.83	1.0035
3H5-02	1397.12	1.0051
3H5-04	1382.42	0.9945
3H5-05	1388.49	0.9989
3H5-07	1381.03	0.9935
3H5-09	1392.61	1.0019
4H5-01	1380.93	0.9935
4H5-02	1387.47	0.9982
4H5-04	1389.15	0.9994
4H5-05	1389.34	0.9995
4H5-07	1384.10	0.9958
4H5-09	1394.73	1.0034
5H5-01	1388.26	0.9987
5H5-02	1385.35	0.9967
5H5-04	1398.03	1.0058
5H5-05	1393.07	1.0022
5H5-07	1393.15	1.0023
5H5-09	1393.60	1.0026
STDEV	5.35	0.0039

2.4 IC Analysis

To increase the concentration accuracy in IC analysis, higher sampling weights were employed in extracting the acidic and ionic species. Differing from extraction method in the previous work[7], 90 mg of NP samples were used in the liquid-liquid extraction (LLE) with 30 mL total of LCMS

grade water (i.e., 3 repeated LLE using 10 mL H_2O each). The accuracy of HNO_3 measurements was assessed using duplicate measurements of the time zero samples (i.e., unaged, labelled as 00A and 00B). On the other hand, the accuracy of HONO measurement was assessed using the blank and spiked samples of 3H4-06. The nitrite solution or spike solution was prepared by dissolving 9.8 mg of sodium nitrite in 10 mL water, of which 9.18 µL was added to the prepared extract of 3H4-06 sample to give a final spike concentration of 0.2 ppm.

Separation of anions sample was done on a Dionex ICS-2100 instrument (Thermo Fisher Scientific Inc., USA) following EPA method 300.0[17]. The column is a Dionex IonPac AS15 (Thermo Scientific, Waltham, MA, Prod. # 053941). Mobile phase is made using an Eluent Generator Cartridge, Dionex ECG III KOH RFIC (Thermo Scientific, Waltham, MA, Prod. # 074532) at a 38 mM KOH concentration using DI water with a flow rate of 0.4 mL /min. The IC system has a conductivity detector. Undiluted and 1:10 diluted samples using DI water obtained from MilliQ system were analyzed. Complete chromatographic resolution cannot be achieved between formate and acetate ions due to column separation limitations[18], thus both ions are combined as a sum and denoted as acetic/formic hereinafter. The concentrations of HONO, HNO_3, acetic/formic, and oxalic acids were quantified using their anionic forms. The calibration standards include Nitrite (0.5-5.0 ppm), Nitrate (2.0-20.0 ppm), Oxalate (0.5-5.0 ppm), and Acetate (0.1-1.0 ppm).

2.5 LC-QTOF Analysis

50 mg of NP samples were dissolved in 10 mL of ACN (I) for analysis using a SCIEX ExionLC system coupled with X500R QTOF tandem mass spectrometry instrument. Undiluted LC-QTOF samples were injected to maximize intensities of low abundant degradants, such as 2,2-dinitropropanol (DNPOH). Data were collected using information dependent acquisition (IDA) in both positive and negative electrospray ionization (ESI+ and ESI-) at a MS scan range of precursor ions (MS spectra) from 80 to 650 Da with dynamic background subtraction. Based on the I blank injections, the exclusion lists of interference ions for both ESI+ and ESI- were obtained and applied. A threshold of 200 cps was selected for trigger of fragment ion spectra (MS/MS) with ≤30 and ≤20 candidate precursor ions per cycle, in the ESI+ and ESI- modes, respectively, which gave a cycle time of 1.726 s (869 cycles) and 2.193 s (1759 cycles). The TOF MS and MS/MS accumulation times were set to 100 and 50 ms, respectively. The declustering potentials were set to +50 V or -40 V respective to polarity. The collision energies were set to 26 ± 15 V in ESI+ and -25 ± 20 V in ESI- for the QTOF MS/MS experiments. Chromatography was achieved with Kinetex C8 reverse phase column (2.6 µm, 150 x 3.0 mm) held at 35°C. For the chromatographic run in ESI+ mode, a linear gradient from 40 to 75% (0 to 20 min) organic at a flow rate of 0.33 mL/min was used with mobile phases of 0.1% formic acid in water and 0.1% formic acid in I. For the chromatographic run in the ESI- mode, a linear gradient from 33 to 85% (0 to 20 min) organic at a flow rate of 0.30 mL/min was used with mobile phases of 0.1% ammonium acetate (NH_4AcO) in water at pH 6 (adjusted with acetic acid) and 0.1% NH_4AcO in 95:5 (v/v) I:MeOH at pH 6. Compared to previous analyses[6], there are several changes in the LC and MS methods for analyzing more concentrated extracts (i.e., 5000 mg/L instead of 300 mg/L): 1) expanded duration

of gradient, from 10 min to 20 min, to provide better separation of compounds; 2) lower declustering potentials, from +80 V to +50 V in positive mode and from -80 to -50 V in negative mode, to reduce insource fragmentation[19, 20]; and 3) increased number of candidate precursor ions per cycle (e.g., 30 or 20 ions instead of 4 ions) to enrich MS/MS spectrometric information[19, 21, 22].

2.6 Karl Fischer (KF) Titration

KF titration was used to determine water concentrations in the NP samples using a Mettler Toledo compact coulometric titrator (model C30S). Samples were analyzed mostly in triplicate (duplicate when samples required high volumes or highly exceeded the concentration quantification limits of the instrument) with injection volumes of 0.1 and 0.3 mL based on the concentration of water in the samples. The KF solution (Honeywell Coulomat A and CG) was changed prior to each day of analysis, equilibrated, and tested in triplicate against 100, 1000, and 10000 ppm water standards in xylenes (Supelco).

2.7 Fourier Transform Infrared Spectroscopy (FTIR)

A Thermo Nicolet™ iS50 FTIR spectrometer was used to perform the FTIR measurement in an attenuated total reflectance (ATR) mode with a diamond crystal between 4000 and 450 cm^{-1}. The resolution of 4 cm^{-1} and 16 scans were used. Thermo OMNIC™ software was used to process the results. For each sample, two to four spectra were collected and the average spectrum was used for data analysis.

3. Results and Discussion

3.1 Accuracy Assessment of IC Measurements

The measured concentrations of added HNO_3 at time zero for each treatment type of NP samples are summarized in Tables 14. The accuracies of the determined HNO_3 concentrations are between 95 to 115% (in green), demonstrating that the added HNO_3 are fully homogenized with the NP samples. As expected, compared to their concentrations at NP hydrolysis in Table 15, other acidic species besides HNO_3 are at least a magnitude lower in concentrations. Unlike the concentration of acetic/formic acid, the concentrations of HONO and oxalic acid are below 300 μM, meaning that the CVs of 34.11% in oxalic acid and 13.90% in HONO are likely attributed to the instrumental precision error of IC, which is expected in low concentration measurements. Based on the measured difference between the blank 3H4-06 (0.134 ppm) and spiked 3H4-06 (0.340 ppm) samples, the accuracy in HONO measurements is determined at 103%. The precision and accuracy in measurements of oxalic acids are less of a concern because its production only greatly increases in the later stage of NP degradation[7].

Table 14. Acid concentrations in duplicates of treated NP samples at time zero by IC analysis.

Time Zero Samples	HONO Conc. (µM)	HNO_3 Conc. (µM)	Oxalic Acid Conc. (µM)	Acetic/Formic Conc. (µM)	Expected Conc. of added HNO_3 (µM)	Actual conc. of added HNO_3 (µM)	Accuracy (%)
TA9-00A	153	398	52	7527	N/A	N/A	N/A
TA9-00B	208	361	149	6760	N/A	N/A	N/A
C-00A	163	372	136	7140	N/A	N/A	N/A
C-00B	178	395	264	7127	N/A	N/A	N/A
P-00A	134	349	147	8034	N/A	N/A	N/A
P-00B	159	372	126	8382	N/A	N/A	N/A
PH-00A	164	1739	166	8739	1400	1355	**96.81**
PH-00B	156	1741	82	6920	1400	1358	**96.98**
H1-00A	158	767	90	8083	350	384	**109.59**
H1-00B	176	785	91	7779	350	402	**114.83**
H2-00A	137	1140	45	8556	700	756	**108.00**
H2-00B	179	1127	92	7494	700	744	**106.24**
H3-00A	218	1518	69	7978	1050	1134	**108.04**
H3-00B	225	1456	94	7301	1050	1072	**102.11**
H4-00A	229	1721	99	7952	1400	1338	**95.56**
H4-00B	185	1746	110	6822	1400	1362	**97.29**
H5-00A	159	1742	122	8182	1400	1359	**97.06**
H5-00B	232	1763	155	8096	1400	1380	**98.55**
CV (%)	13.90	N/A	34.11	5.34	N/A	N/A	N/A

All acidic species are measured as anions in IC.

Table 15. Reference acid concentrations at NP hydrolysis determined in the previous experiment.

Sample Name	Aging Months	HONO Conc. (µM)	HNO_3 Conc. (µM)	Oxalic Acid Conc. (µM)	Acetic/Formic Conc. (µM)	DNPOH (µM)
5A-33	**32.9**	3494	791	4569	187230	327008
6A-18	**18.7**	14482	5030	3823	173599	376668

3.2 Assessment of Water Concentration at Time Zero

Table 16 shows the loss of water as a function of time using the KF measurements of the inert NP and TA-9 NP samples. In the treated TA-9 NP samples at time zero, the water concentrations are further decreased and yielded an average of 245 ± 16 ppm, which are far less than the expected concentration of 961 ppm (estimated in Section 2.2.3). Compared to the difference between sample 8 and the average of samples 9-16, the loss of 95 ppm of water is likely attributed to the evaporation in the large headspace of 600-mL beaker and prolonged duration of stirring.

Table 16. Measured water concentrations by Karl Fischer (KF) titration.

Sample No.	Sample information	Sample Type	H_2O conc. (ppm)
1	measured in 07/2017	**Inert NP**	784
2	measured in 10/2017	**Inert NP**	627
3	measured in 02/2018	**Inert NP**	544
4	measured in 01/2023	**Inert NP**	624
5	not homogenized, measured in 07/2017	**TA-9 NP**	546
6	not homogenized, measured in 10/2017	**TA-9 NP**	474
7	not homogenized, measured in 02/2018	**TA-9 NP**	353
8	not homogenized, measured in 01/2023	**TA-9 NP**	339
9	0 μM HNO_3, homogenized TA-9 NP	**C**	233
10	350 μM HNO_3	**H1**	248
11	700 μM HNO_3	**H2**	276
12	1050 μM HNO_3	**H3**	243
13	1400 μM HNO_3	**H4**	236
14	1400 μM HNO3, heated	**H5**	260
15	PBNA	**P**	228
16	PBNA + HNO_3	**PH**	234
		Average conc. between samples 9-16	245 ± 16

3.3 Semi-quantitative Search for Significant Unknowns

3.3.1 Heatmap Assessment

Figure 6 presents a total of 34 unknowns found in all treatment types of NP samples, where each is given by a unique m/z and retention time. The heatmap is divided into two panels: ESI+ and ESI-. The m/z values are arranged in the order of increasing retention time. Each individual box of the heatmap represents a CV value, which illustrate the relative change of intensity in the found m/z across 21 weeks of aging in each temperature for each treatment type. Based on the vertical alignment of CVs, the greatest changes are observed in the ESI+ data, including m/z of 247.0868 (7.98 min), 219.1047 (10.30 min), 249.1027 (10.30 min), 435.1855 (16.83 min) and 436.1918 (18.93 min). On the other hand, the changes in m/z found in the ESI- data are much less significant (CV < 31.60%). Among the significant m/z, the changes in m/z 247.0868 is minimal in response to the different types of treatment and temperature effect; compared to acid addition, m/z 435.1855 and 436.1918 exhibit a greater change when PBNA is added (P and PH) and both m/z are temperature sensitive; both m/z 219.1047 and 249.1027 are very responsive to the temperature change, acid and/or PBNA additions. Based on their shared retention time of 10.30 min and nearly identical colors across all calculated CVs, m/z of 219.1047 and 249.1027 are identified as daughter and parent ions of the same compound, which is discussed in detail in the following sections. This map also provides evidence that ESI+ results are more informative than the ESI- results.

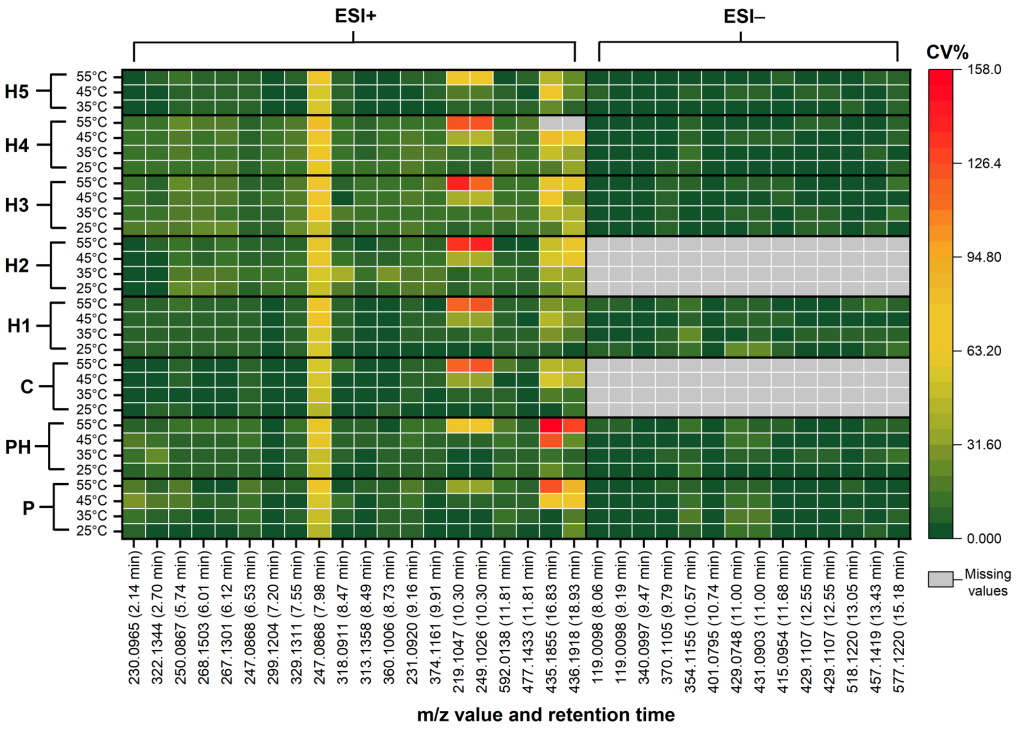

Figure 6. Heatmap of abundance changes, represented by CV values, in found m/z (x-axis) for all temperatures of all treatment types (labelled on y-axis). Due to instrumental issue in ESI- mode, the measurements of C and H2 were not obtained, but the missing values (in gray) do not affect our data interpretation.

3.3.2 Changes Associated with PBNA Addition

Figure 7 shows the mean intensities (%, calculated by the mean of measurements obtained from all temperatures for each treatment divided by the mean of measurements obtained from all temperatures of all three treatments) of the 34 unknowns. To compare the difference in PBNA addition between with and without the added HNO_3 (1400 µM), only C (or H1), P, and PH samples are displayed. All intensity differences are very subtle except for m/z 230.0965 (2.14 min), 322.1344 (2.70 min), 250.0867 (5.74 min), 219.1047 (10.30 min), 249.1027 (10.30 min), 435.1855 (16.83 min) and 436.1918 (18.93 min), which confirms the effect of PBNA addition observed in Figure 6 on these four m/z species. Furthermore, the added HNO_3 significantly increases the formation of m/z 435.1855 and 436.1918. Yet again, the m/z species found in ESI- show no significant difference and thus they are omitted in further analysis.

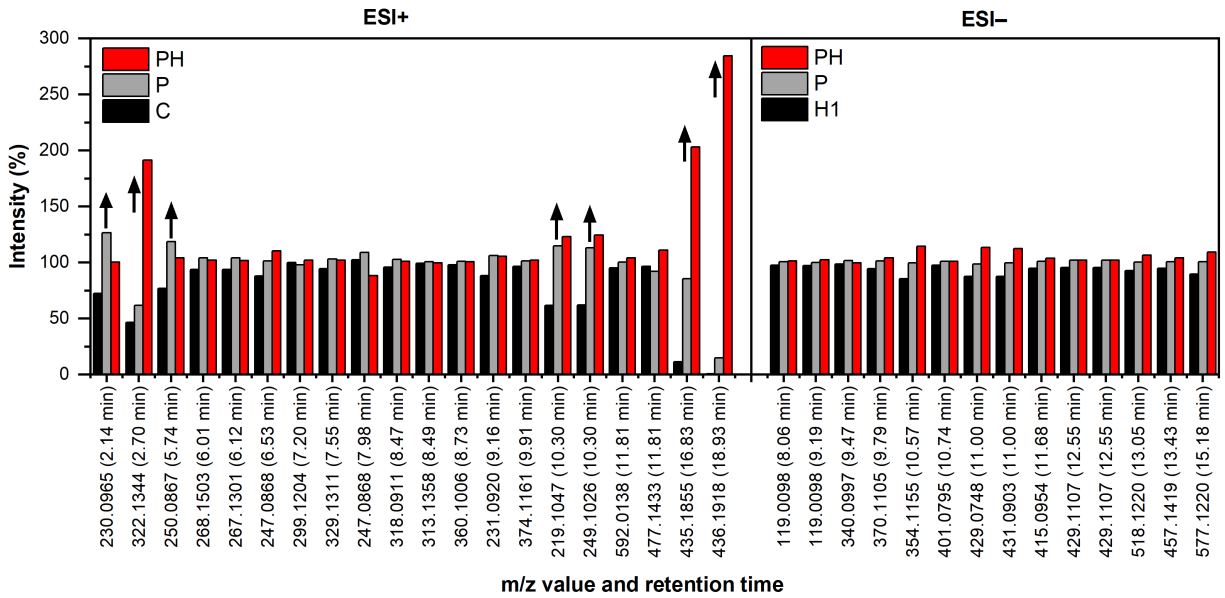

Figure 7. Comparison of unknowns between untreated or minimally acidified NP (C or H1), NP treated with PBNA (P), and NP treated with both PBNA and HNO_3 (PH). The mean intensities are taken from measurements across 21 weeks of aging of all temperatures. Because of the missing ESI- data in C and H1 shows similar results in ESI+ mode, H1 is used in placed of C for ESI- comparison.

3.3.3 Changes Associated with HNO_3 Concentration

Table 17 presents the mean intensities of all temperatures for ESI+ unknowns in the 21-week-aged untreated and acidified NP samples, including C (0 μM), H1 (350 μM), H2 (700 μM), H3 (1050 μM), and H4 (1400 μM). To assess whether the intensity changes in each unknown is associated with HNO_3 concentrations, the corresponding CVs are calculated, and the coefficients of determination (r^2) are determined from the linear regression between the mean intensities and HNO_3 concentrations. For values that are highlighted in red, either the intensity changes are obvious (CV > 15%) or the r^2 value shows good reliability (i.e., $r^2 > 0.9$; high degree of correlation and agreement between measurements)[23]. In m/z 268.1503 (6.01 min) and 267.1301 (6.12 min), the r^2 values demonstrate good reliability but the CVs are too low to be significant, which is also observed in Figure 6 (i.e., only green colors shown on the vertical alignment). In m/z 247.0868 (6.53 min), while a large change in intensities is observed, the degree of linear correlation is only moderate, and its mean intensities are relatively low (10^4 cps^2) compared to most unknowns (>10^5 cps^2). The mean intensities of m/z 435.1855 (16.83 min) and 436.1918 (18.93 min) are also very low (10^3 and 10^2 cps^2) though their CVs are large with reasonable r^2 values. Among all m/z species, m/z 219.1047 and 249.1027 species exhibit very strong signals (10^7 cps^2), large CVs, and excellent r^2 values (> 0.90), which indicates their changes are very significant and strongly correlated with the HNO_3 concentration.

Table 17. Effect of HNO_3 addition after 21 weeks of aging.

m/z and Retention Time	C, 0 µM HNO_3	H1, 350 µM HNO_3	H2, 700 µM HNO_3	H3, 1050 µM HNO_3	H4, 1400 µM HNO_3	CV%	Linear Regression (r^2)
230.0965 (2.14 min)	525384	513506	551343	534132	529805	2.60	0.114
322.1344 (2.70 min)	203865	192254	211158	204303	207778	3.50	0.194
250.0867 (5.74 min)	208390	220636	208876	216035	218227	2.58	0.185
268.1503 (6.01 min)	568094	583897	590014	608965	620544	3.49	**0.984**
267.1301 (6.12 min)	160832	166393	164424	169815	172578	2.75	**0.863**
247.0868 (6.53 min)	4537425	4587249	4798619	4774831	4753280	2.54	0.675
299.1204 (7.20 min)	5831517	5719254	5741023	5404771	5504589	3.16	0.739
329.1311 (7.55 min)	249638	269740	265005	253033	254706	3.30	0.015
247.0868 (7.98 min)	56613	31705	26626	23250	25258	**42.01**	0.671
318.0911 (8.47 min)	272582	284902	290413	346694	337729	10.90	0.194
313.1358 (8.49 min)	2192061	2296690	2257472	2112912	2082510	4.18	0.486
360.1006 (8.73 min)	499487	514084	505696	464324	457190	5.26	0.685
231.0920 (9.16 min)	767689	788046	755186	795385	791420	2.22	0.251
374.1161 (9.91 min)	207910	218854	200894	190013	190532	6.05	0.680
219.1047 (10.30 min)	937647	880331	767003	654707	510198	**23.01**	**0.981**
249.1027 (10.30 min)	2143906	2039108	1796674	1530734	1207829	**21.89**	**0.972**
592.0138 (11.81 min)	514049	518532	524573	512784	497983	1.92	0.368
477.1433 (11.81 min)	295393	242221	309912	248665	235777	12.69	0.278
435.1855 (16.83 min)	1774	1544	1025	999	1056	**27.88**	**0.773**
436.1918 (18.93 min)	676	718	373	285	243	**48.57**	**0.850**

3.4 Identification of Nitroso-PBNA

As summarized in Section 3.3, the most pronounced correlation with PBNA addition and HNO_3 concentration in the ANTA experiment is found in m/z 249.1027 (10.30 min) and 219.1047 (10.30 min). Given by their similarities in retention time and peak shape and the common m/z at 219, 218, 217, 116, 115 and 66 in Figure 8, m/z 219.1047 is confirmed as the insource fragment of m/z 249.1027. The m/z 219.1047 was originally detected in our 44-month aged NP samples and initially speculated as an interference because its intensity profile was not carefully examined[6]. Additionally, m/z 249.1027 is not detected using the previous MS method (high voltage selected, +80V) due to insource fragmentation. By lowering DP in ESI+ mode, m/z 249.1027 is finally detected in the ANTA samples. Through structural elucidation of the fragment ions, as shown in Figure 9, we accurately identified m/z 249.1027 as nitroso-PBNA (PBNA-NO).

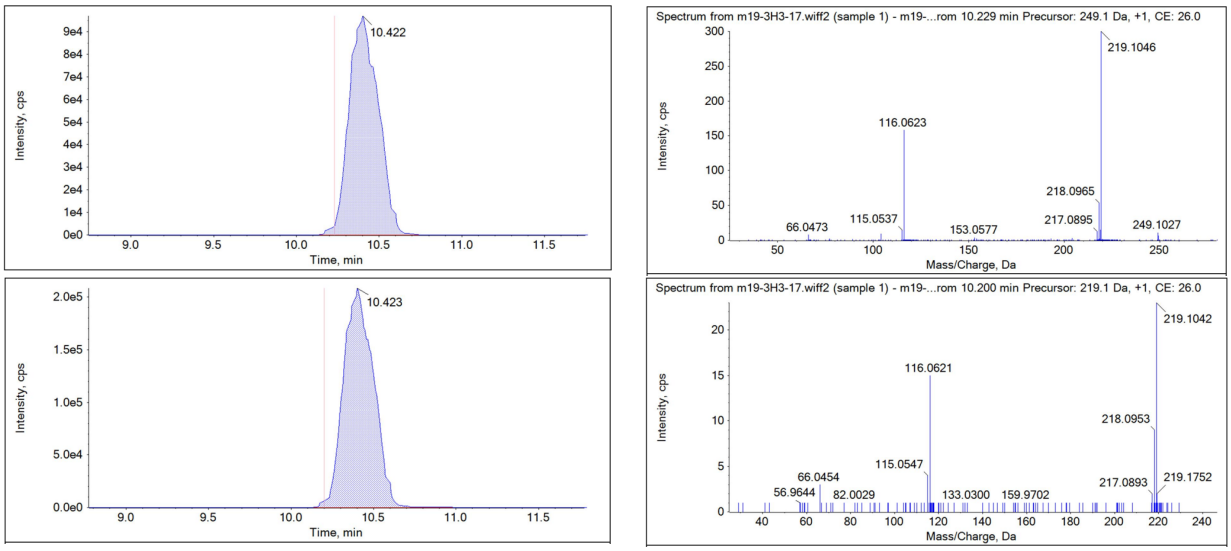

Figure 8. Comparison of peak shape (left) and fragment ion spectra (right) of m/z 249.1027 (top) and 219.1047 (bottom). The spectra are obtained from ANTA sample 3H3-17.

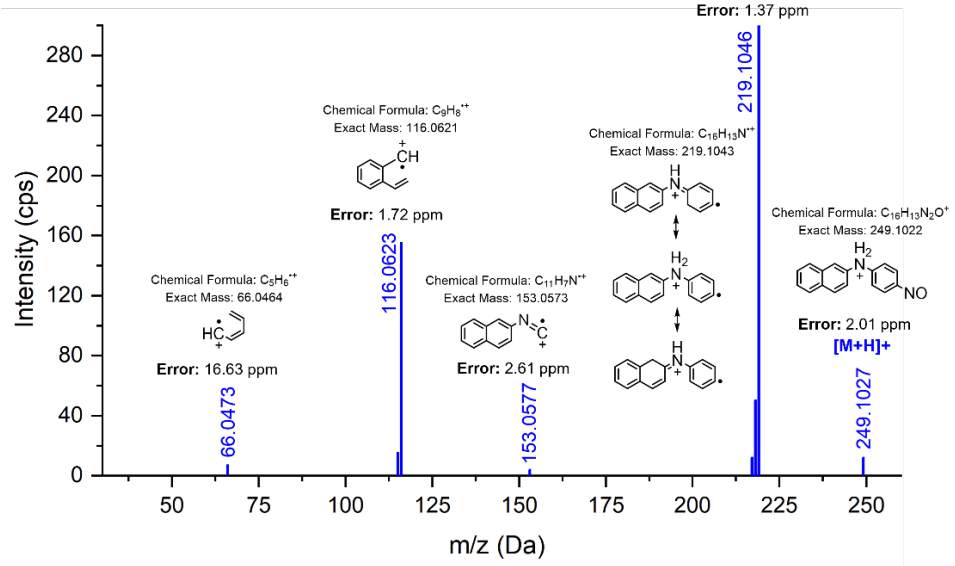

Figure 9. Verification of nitroso-PBNA via elucidation of fragment ion spectrum of ANTA sample 3H3-17. The m/z 66.0473 has a slightly higher mass error because it is outside of the mass calibration range.

The characteristics of large abundance (e.g., very strong signal) and high sensitivity towards the various experimental conditions in the ANTA experiment as such indicate that the m/z 249.1027 (nitroso-PBNA) is a crucial compound in the early stage of NP degradation. Therefore, we prioritized our focus on nitroso-PBNA, whereas the m/z values with lesser significance, including 435.1855 (16.83 min), 436.1918 (18.93 min), 247.0868 (7.98 min), 230.0965 (2.14 min), 322.1344 (2.70 min), and 250.0867 (5.74 min), have been archived for future analysis. It is worth noting that the m/z 435.1855 and 436.1918 species are likely dimers of PBNA based on their plausible chemical formulas of $C_{32}H_{23}N_2^+$ and $C_{32}H_{24}N_2^+$, respectively.

3.5 Role of Nitroso-PBNA

Figure 10 presents the concentration profiles of HNO_3, HONO, PBNA, PBNA-NO, mononitro-PBNA (PBNA-NO_2), and PBNA-$2NO_2$ over 21 weeks in the P and PH set of samples at 25, 35, 45 and 55°C. The changes in PBNA and PBNA-NO are most pronounced in the P and PH set of samples due to the PBNA addition. As PBNA depletes, PBNA-NO forms. Their aging trajectories mirror each other across all temperatures, which indicates an apparent reactant-product relationship. The direct conversion of PBNA to PBNA-NO requires a source of nitrosonium ion (NO^+) and can be supplied through HONO reacting with a strong acid (e.g., HNO_3, HCl, H_2SO_4, etc.), which produces H_2O as a byproduct, as shown in Scheme 1.

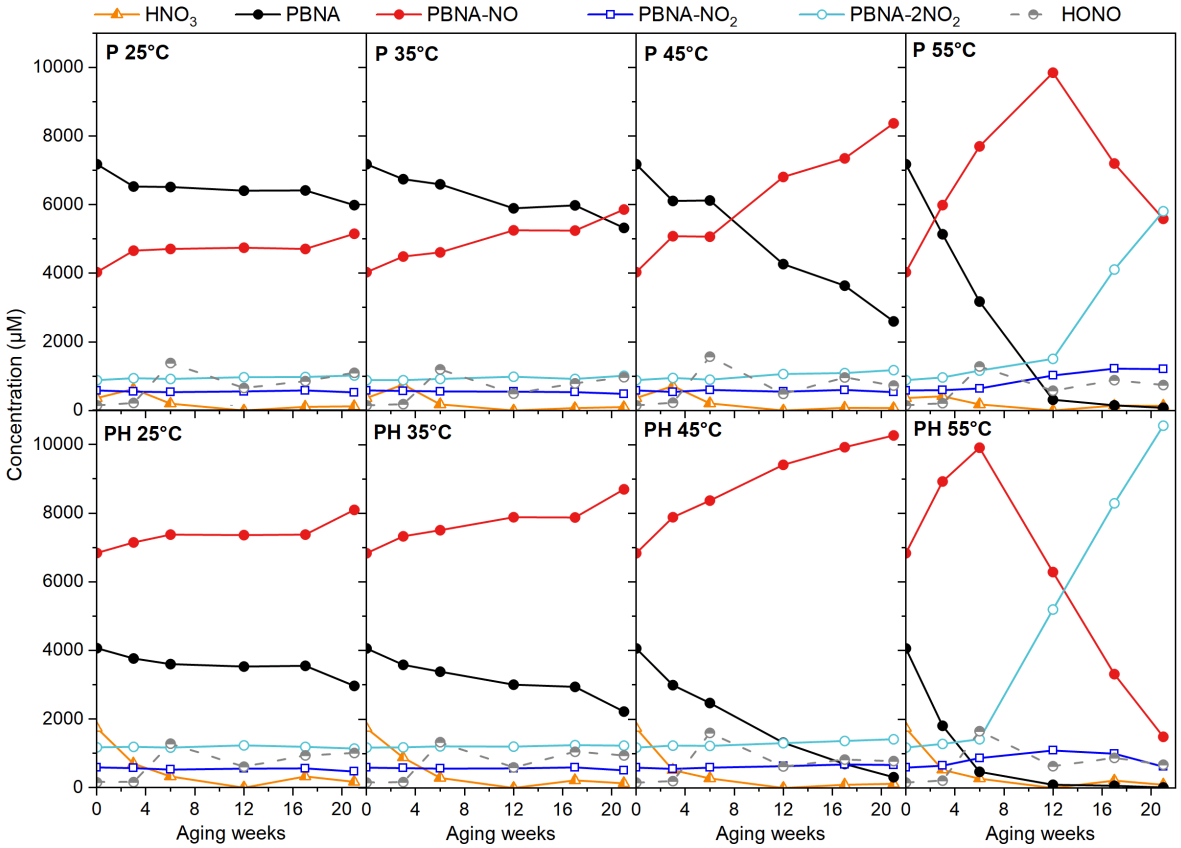

Figure 10. Time evolution of HNO_3, PBNA, PBNA-NO, PBNA-NO_2, PBNA-$2NO_2$, and HONO in the P and PH set of samples over 21 weeks of aging at 25, 35, 45 and 55°C.

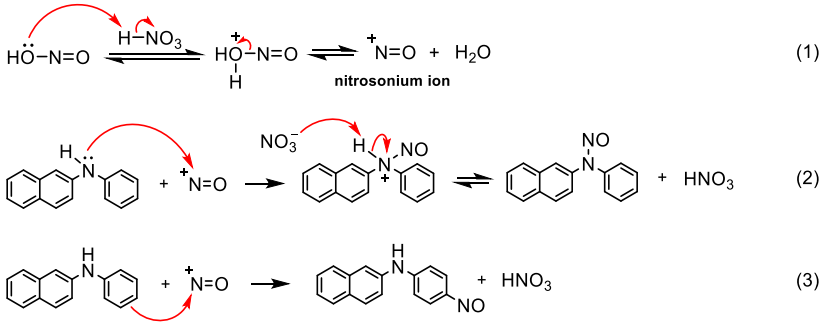

Scheme 1. Nitrosation via HONO catalyzed by strong acid (e.g., HNO_3).

In the case of PH, the added HNO_3 can be conveniently used in the proton transfer reaction. This nitrosation mechanism is a classic reaction of a secondary arylamine with nitrous acid, which generates nitrosoamine (typically N-N attachment)[24]. However, the exact position of NO is attachment cannot be specified from the fragment ion spectrum. While intramolecular rearrangement may displace the NO group to a different position on the PBNA rings (e.g., Fischer-Hepp rearrangement)[25, 26], the bulky ring structures in PBNA may block the approach of NO^+ through the N-N attachment[27]. Based on the DFT prediction and experimental evidence of where NO_2^+ ion is positioned in mononitro-PBNA[15], the NO-addition at the ortho position is highly plausible. As depicted in Scheme 1, HNO_3 is served as a catalyst in the nitrosation reaction. Because of the additional 1400 μM of HNO_3, the reaction rate of converting PBNA and PBNA-NO is increased, which results in more PBNA-NO than PBNA in PH set of samples than in the P set of samples. However, HNO_3 are also consumed through other competitive reactions, such as nitration. It is worth noting that other strong acids can also induce the same catalysis, such as HCl and H_2SO_4, which are previously detected though their concentration profile shows no correlation with the degradation of NP or PBNA[7].

The concentration changes in HNO_3, HONO, PBNA-NO_2, and PBNA-$2NO_2$ are minimal (<2000 μM) at 25, 35, and 45°C. At the 12th week of aging in the P set of samples and the 6th week of aging in the PH set of samples at 55°C, when PBNA are consumed to an extremely low concentration and as PBNA-NO reaches its maximum, the formation of PBNA-NO_2 and PBNA-$2NO_2$ rapidly increases, perhaps due to nitration or oxidation or combination of both. Like the PBNA and PBNA-NO pairs, the PBNA-NO and PBNA-$2NO_2$ pairs also shows a mirror image of their concentration change, which indicates: 1) nitro-substituted PBNAs are originated from PBNA-NO and thus nitrosation is a preceding event to nitration; and 2) PBNA-$2NO_2$ is the primary product that derived from PBNA-NO. However, we cannot discern whether the nitration event is HONO driven ($NO_2^{\bullet}$) or HNO_3 driven (NO_2^+) because the HONO concentration has a wavy trajectory and HNO_3 concentration only decreases over time. As depicted in Schemes 2 and 3, nitroso compounds can be oxidized into nitro compounds in the presence of NO_2[28], and nitro compounds can also be produced from nitration via NO_2^+[9, 10], which both scavenging mechanisms consumes HNO_3. Perhaps for this reason, HNO_3 concentration decreases over time. Simultaneously, HONO are being generated and scavenged over time, resulting in a wavy trajectory of concentration change. Furthermore, a faster growth of PBNA-$2NO_2$ at much higher concentration than PBNA-NO_2 suggest the progression of nitration is very rapid. In contrast to the P set of samples, a faster transition from nitrosation to nitration in the PH samples is attributed to the addition of HNO_3. Hence, a higher HNO_3 concentration promotes the reaction efficiency of both nitrosation and nitration.

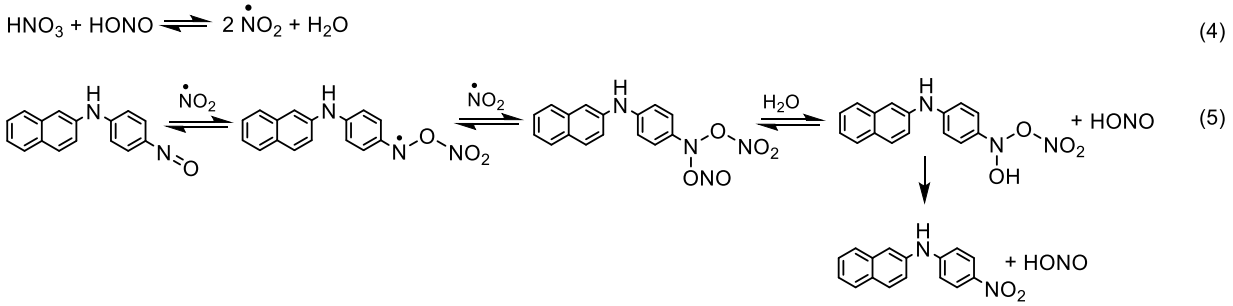

Scheme 2. Oxidation of Nitroso-PBNA.

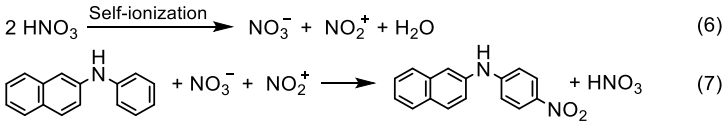

Scheme 3. Self-ionization of HNO_3 and nitration via NO_2^+.

Figures 11 to 14 shows the concentration profiles of HNO_3, PBNA, PBNA-NO, PBNA-NO_2, PBNA-$2NO_2$ and HONO over 21 weeks in C and H1 to H4 set of samples at 25, 35, 45 and 55°C. As shown at time zero, majority of PBNA (≤ 81 µM or 0.002 wt.%) in the TA-9 NP had been converted to PBNA-NO, which confirms that nitration primarily occurs after nitrosation. The promotion of nitration by HNO_3 is demonstrated by the decreasing initial concentration of PBNA-NO and increasing initial concentrations of PBNA-NO_2 and PBNA-$2NO_2$ as HNO_3 increases from 0 to 1400 µM. The rate of nitration appears to be approximately the same regardless of HNO_3 concentration because the role of HNO_3 is changed from being a catalyst to being a source of NO_2^+ ion. However, the rate of nitration does increase noticeably as temperature increases because the elevated temperatures can potentially create a more dehydrated environment due to water evaporation into the headspace, which promotes self-ionization of HNO_3 into NO_3^- and NO_2^+ ions [10]. In the formation of PBNA-$2NO_2$, both PBNA-NO and PBNA-NO_2 decreases in concentration, which suggests that the oxidation of PBNA-NO and the sequential nitration can occur simultaneously. Because of this rapid progression of nitration toward the formation of PBNA-$2NO_2$, the concentration of PBNA-$2NO_2$ is always greater than the concentration of PBNA-NO_2 in all samples, which also agrees with the results obtained from the 44-month aging experiment[6].

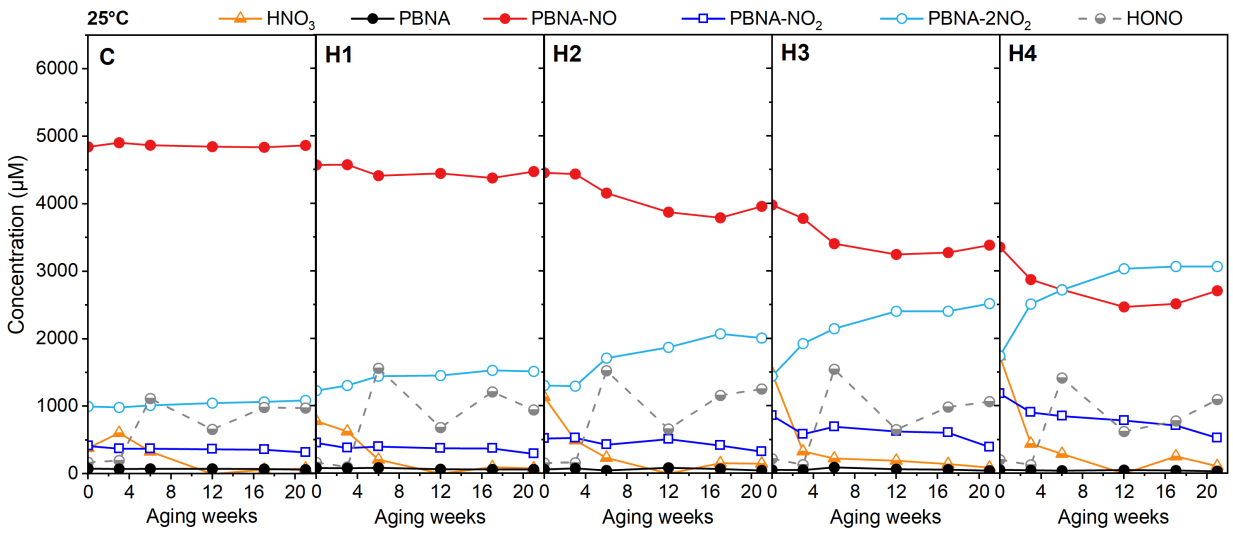

Figure 11. Time evolution of HNO_3, PBNA, PBNA-NO, PBNA-NO_2, PBNA-$2NO_2$, and HONO in the C and H1 to H4 set of samples over 21 weeks of aging at 25°C.

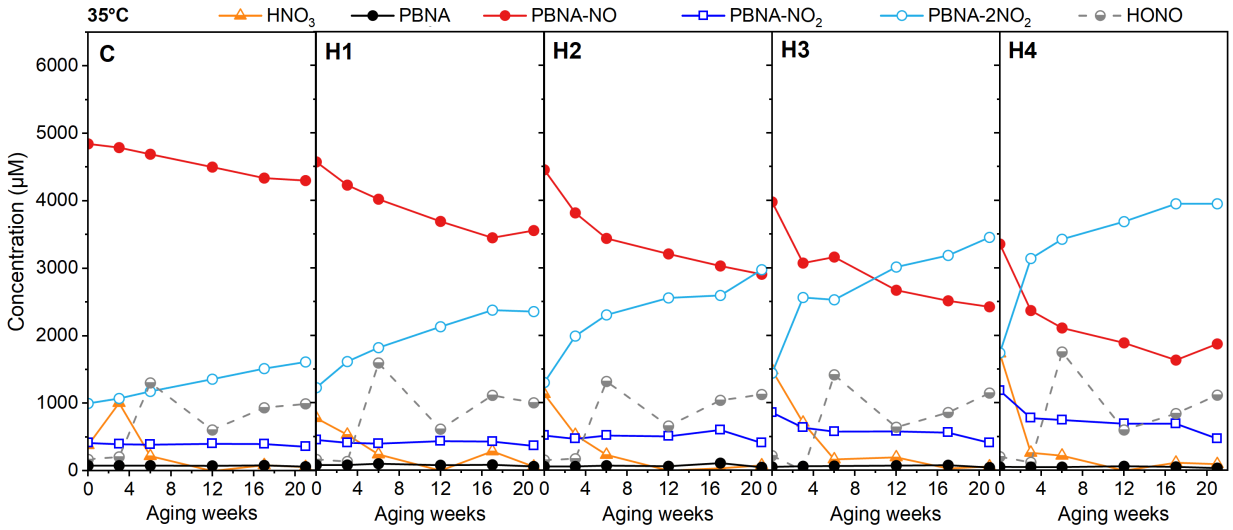

Figure 12. Time evolution of HNO_3, PBNA, PBNA-NO, PBNA-NO_2, PBNA-$2NO_2$, and HONO in the C and H1 to H4 set of samples over 21 weeks of aging at 35°C.

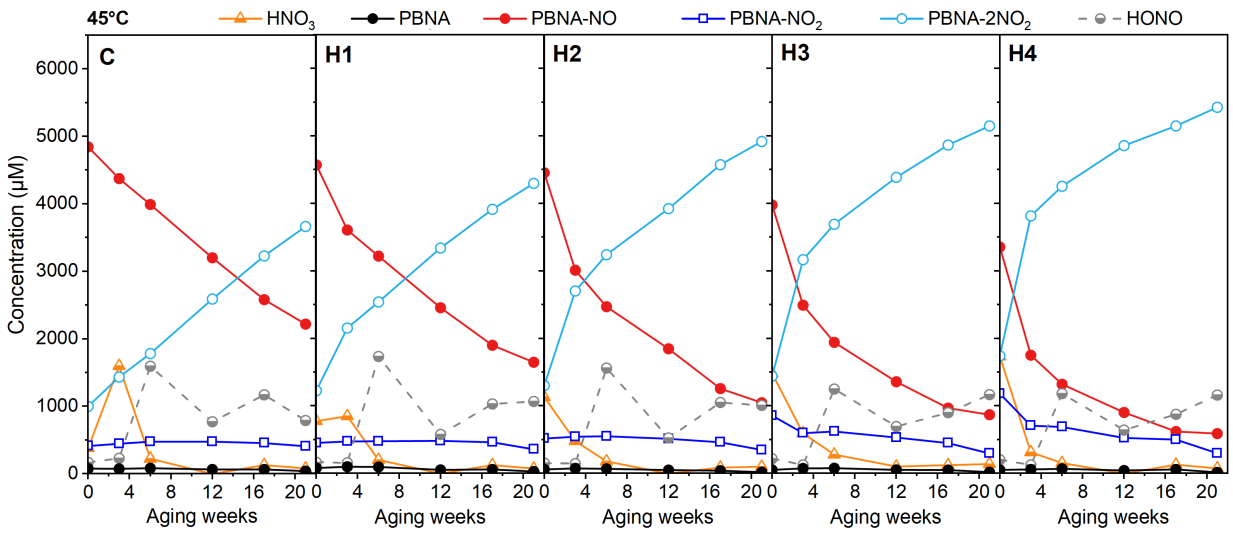

Figure 13. Time evolution of HNO_3, PBNA, PBNA-NO, PBNA-NO_2, PBNA-$2NO_2$, and HONO in the C and H1 to H4 set of samples over 21 weeks of aging at 45°C.

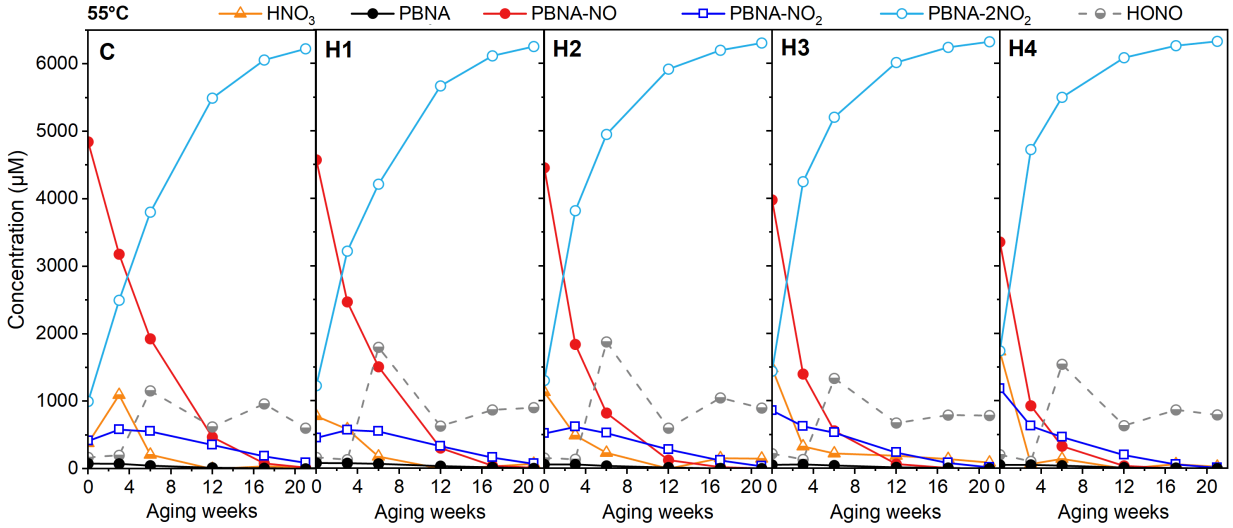

Figure 14. Time evolution of HNO_3, PBNA, PBNA-NO, PBNA-NO_2, PBNA-$2NO_2$, and HONO in the C and H1 to H4 set of samples over 21 weeks of aging at 55°C.

Figure 15 shows the intensity profile of trinitro-PBNA (PBNA-$3NO_2$) in the P, PH, H1, H3 and H4 set of samples at 25, 35, 45 and 55°C. As the initial HNO_3 concentration increases from 350 (in H1) to 1400 μM (in H4), the relative abundance of PBNA-$3NO_2$ increases. In the presence of added PBNA (P and PH), the progression of nitration is delayed and thus less PBNA-$3NO_2$ are produced in the PH set of samples (1400 μM), despite the HNO_3 concentration is higher in the PH set of samples than the H1 set of samples (350 μM). Without the addition of HNO_3, the formation of PBNA-$3NO_2$ becomes even less significant, which demonstrates the importance of PBNA and PBNA-NO in protecting NP from HNO_3 attack and the addition of PBNA in preventing the nullification of PBNA species.

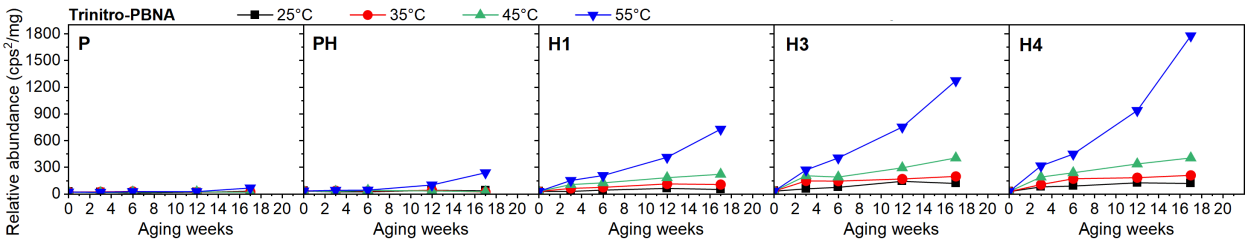

Figure 15. Time evolution of trinitro-PBNA in P, PH, H1, H3 and H4 samples over 17 weeks of aging at 25, 35, 45 and 55°C. The measurements of C, H2, and 21-week-aged samples were not obtained because of the instrumental issue in ESI- mode, but the missing values do not affect our data interpretation.

3.6 Complex Equilibrium of HNO_3 and HONO

Figures 16 and 17 present the concentrations of HNO_3 over 21 weeks of aging in all ANTA samples (C, P, PH, H5, H1, H2, H3, and H4). In Figure 16, without the initially added HNO_3 to the C and P set of samples, HNO_3 concentration is increased at week 3 of aging, which could be derived from HONO decomposition (i.e., 4 HONO → N_2O + H_2O + $2HNO_3$)[7]. As HNO_3 are completely consumed at the 12th week, an increase of HNO_3 concentration is observed again though much lower in concentration. In Figure 17, the HONO concentration profiles show an almost identical wavy trajectory across all treatment types of NP samples. These characteristics imply a very complex equilibrium exist between HONO and HNO_3, because their relative abundances in NP are constantly changing due to a suite of reactions involved, such as HONO elimination, HONO decomposition, HNO_3 formation, PBNA nitrosation, and PBNA nitration. It is worth noting that the trajectory of HNO_3 concentration at 35°C of the H5 samples is diverted to a different direction after the 5th week, perhaps the equilibrium of volatiles in the NP phase might have been disrupted because of the accidental heating in an uncontrolled headspace. Therefore, the H5 dataset are only used as reference and omitted in further analysis.

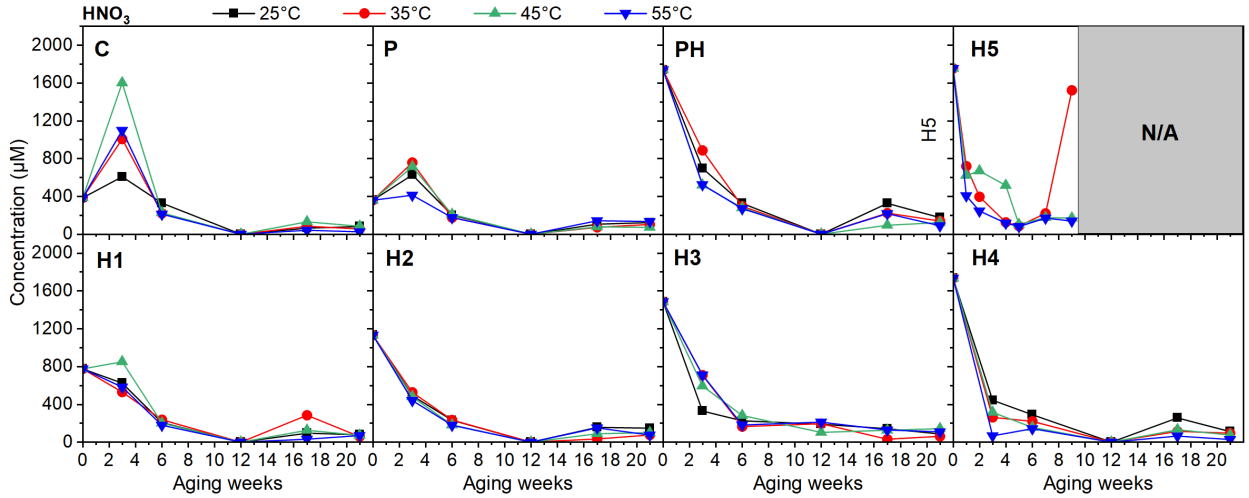

Figure 16. Time evolution of HNO_3 in C, P, PH, H5, H1, H2, H3 and H4 samples over 21 weeks of aging at 25, 35, 45 and 55°C. Because the H5 samples are only aged up to 9 weeks, the area after 9 weeks is voided in grey.

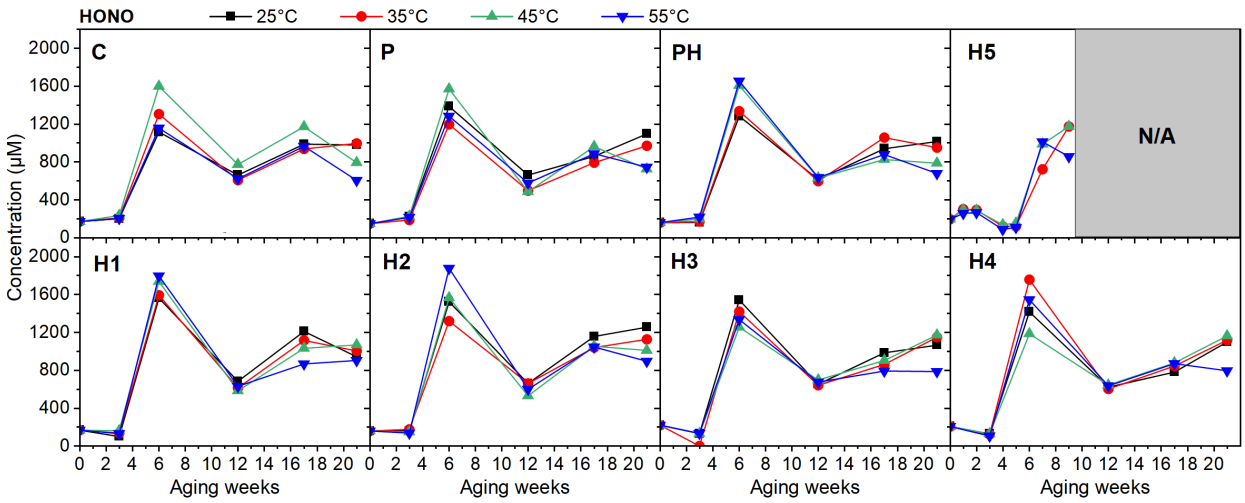

Figure 17. Time evolution of HONO in C, P, PH, H5, H1, H2, H3 and H4 samples over 21 weeks of aging at 25, 35, 45 and 55°C. Because the H5 samples are only aged up to 9 weeks, the area after 9 weeks is voided in grey.

3.7 Measurements of Carboxylic Acids and DNPOH

Figures 18, 19, and 20 present the concentration profiles of acetic/formic acid, oxalic acid, and DNPOH over 21 weeks of aging at 25, 35, 45 and 55°C. Their concentrations are negligibly low compared to those in the 44-month aging experiment and their changes are randomized due to instrumental precision error. This result is expected because the ANTA experiment is a short-term aging study and thus NP degradation stays in its early stage. Without hydrolysis, the acidic species and DNPOH will not form.

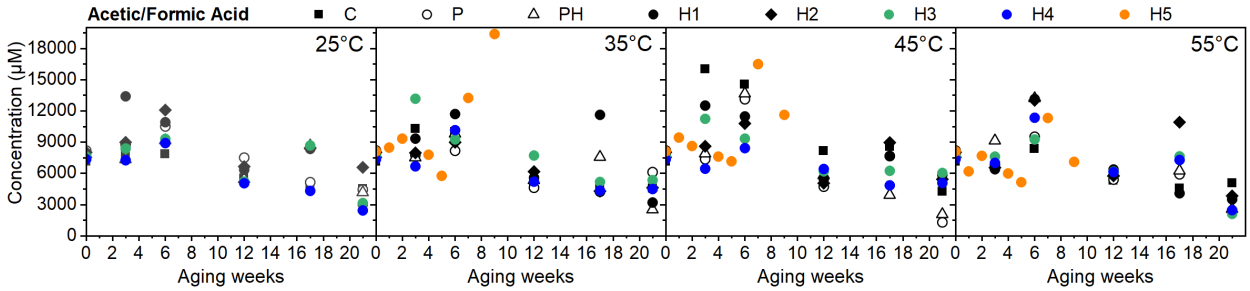

Figure 18. Time evolution of acetic/formic acid in C, P, PH, H5, H1, H2, H3 and H4 samples over 21 weeks of aging at 25, 35, 45 and 55°C.

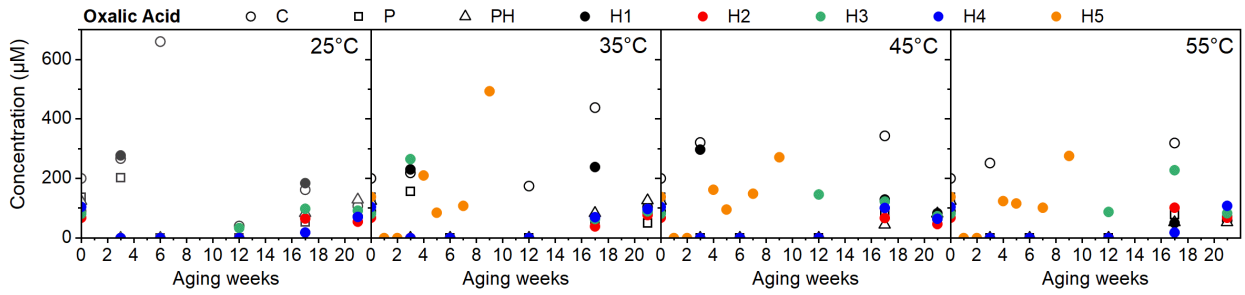

Figure 19. Time evolution of oxalic acid in C, P, PH, H5, H1, H2, H3 and H4 samples over 21 weeks of aging at 25, 35, 45 and 55°C.

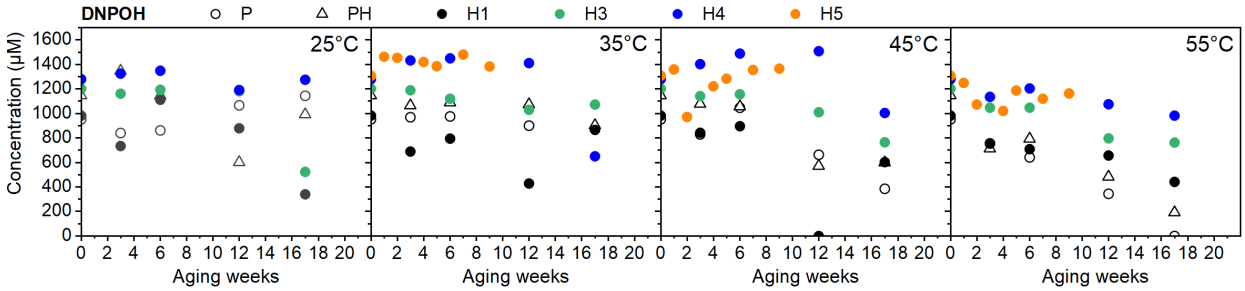

Figure 20. Time evolution of DNPOH in C, P, PH, H5, H1, H2, H3 and H4 samples over 17 weeks of aging at 25, 35, 45 and 55°C. The measurements of C, H2, and 21-week-aged samples were unable to obtain because of the instrumental issue in ESI- mode, but the missing values do not affect our interpretation.

3.8 FTIR Analysis

The insignificant changes are also obtained from the FTIR analysis. As examples, the FTIR spectra of PH and H4 set of samples are compared before and after 21 weeks of aging at 55°C, as shown in Figures 21 and 22, respectively. For better illustration, the FTIR spectra are presented in two regions. Compared to the spectrum of the control sample (C), there are no noticeable changes found in the entire region except for the baseline drafting. Whereas the LC-QTOF vividly detects the changes in the concentration of PBNA, PBNA-NO, and PBNA-xNO_2, these changes are subtle for as measured by the FTIR technique.

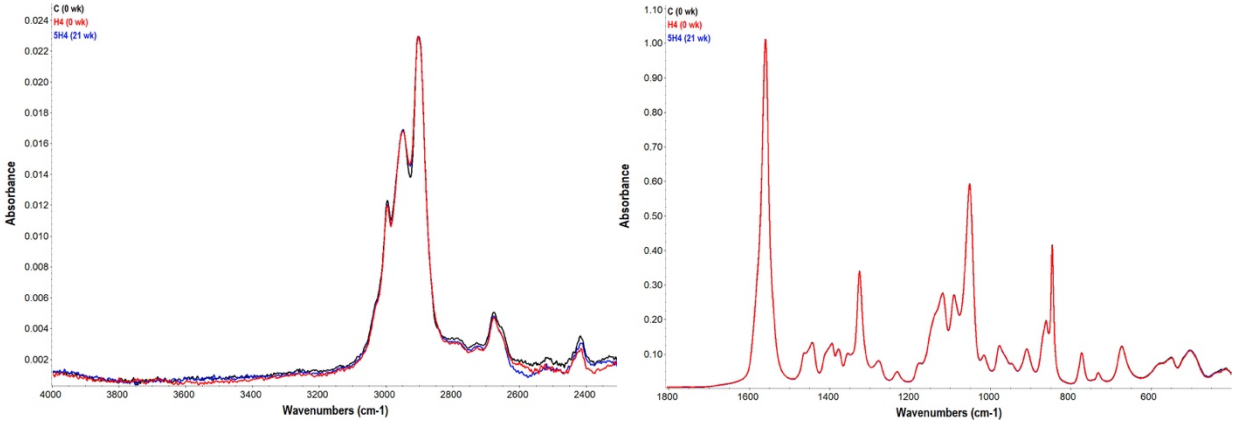

Figure 21. FTIR spectra of control and H4 sample at time zero and H4 sample aged at 55°C for 21 weeks.

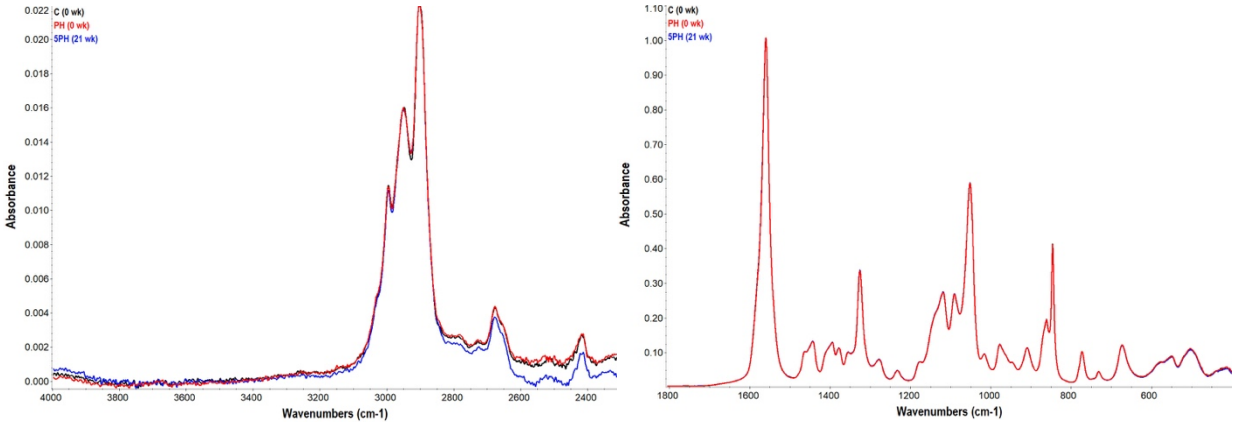

Figure 22. FTIR spectra of control and PH samples at time zero and PH sample aged at 55°C for 21 weeks.

3.9 Kinetic Analysis of PBNA-NO to PBNA-NO_2 and PBNA to PBNA-NO

Because the most pronounced species are PBNA-NO and PBNA-NO_2, whereas the concentration changes in PBNA-NO_2 are more subtle, we bypass PBNA-NO_2 as a transitory species and simplify the reaction to a direct conversion from PBNA-NO to PBNA-NO_2 (A → B, with rate k). The integrated rate law for first order kinetics is,

$$[A](t) = [A]_0 e^{-kt} \; and \; [B](t) = [B]_0 + [A]_0(1 - e^{-kt}) \qquad \textbf{Eq. (5)}$$

These two expressions can be rearranged to define a progress of reaction variable $X_i(t)$ at time t, where $X_i(0) = 1$ and $X_i(\infty) = 0$:

$$X_A(t) = e^{-kt} = \frac{[A](t)}{[A]_0} \qquad \textbf{Eq. (6)}$$

$$X_B(t) = e^{-kt} = \frac{[B]_0 + [A]_0 - [B](t)}{[A]_0} \qquad \textbf{Eq. (7)}$$

If $X_A(t) = X_B(t)$ for all t, then $[A](t)$ and $[B](t)$ are consistent with a first order reaction mechanism.

Using the results from the C samples in the ANTA experiment, this reaction mechanism was tested for the conversion of PBNA-NO to PBNA-$2NO_2$ (Reaction 1). $X_A(t)$ and $X_B(t)$, plotted in Figure 23(left), agree quite well over interval of t = [0, 21] weeks, thus we conclude that the first order mechanism is indeed valid for this reaction. The rate constants k(PBNA-NO) and k(PBNA-$2NO_2$) extracted from an exponential fit of $X_A(t)$ and $X_B(t)$, respectively, are given in Table 18. An Arrhenius fit to the average yields the following:

$$ln[k_{ave}(1)] = 47.400 - 134.222\,x, \; where\; x = \frac{1000}{RT} \; and \; \mathrm{R} = 8.314 \; \frac{J}{mol \times K} \qquad \textbf{Eq. (8)}$$

Also included in Table 18 is a prediction of the rate constant for T = 20°C (estimated T in storage conditions).

Table 18. Rate constants (1/week) for Reaction 1, fit to A = PBNA-NO and B = PBNA-$2NO_2$.

T (°C)	Fit range (weeks)	k(PBNA-NO)	k(PBNA-NO_2)	$k_{ave}(1)$
20	predicted	N/A	N/A	0.00075
35	[0,21]	0.00612	0.00611	0.00611
45	[0,21]	0.03742	0.03803	0.03773
55	[0,6]	0.15363	0.14413	0.14888

Using the results from the P samples in the ANTA experiment, the first order reaction mechanism was tested for the direct conversion from PBNA to PBNA-NO (Reaction 2). For T = 55°C, [PNBA-NO] increases from t = 0 to 6 weeks, starts to slow down at 12 weeks and starts decreasing at 17 weeks. Therefore, for T = 55°C, $X_A(t)$ and $X_B(t)$ was only considered between t = 0 to 6 weeks. $X_A(t)$ and $X_B(t)$, plotted in Figure 23(right), agree quite well over interval of t = [0, 21] weeks for T = 35 and 45°C, and over the interval of t = [0, 6] weeks for T = 55°C. Thus, we conclude that the first order mechanism is indeed valid for this reaction (Note that d[PBNA-$2NO_2$]/dt is small relative to d[PBNA-NO] over these time intervals. Therefore, the contribution from PBNA-$2NO_2$ was neglected). The rate constants k(PBNA) and k(PBNA-NO) extracted from an exponential fit of $X_A(t)$ and $X_B(t)$, respectively, are given in Table 19. An Arrhenius fit to the average yields the following:

$$ln[k_{ave}(2)] = 33.563 - 97.136\,x \qquad \textbf{Eq. (9)}$$

Also, the prediction of the rate constant for T = 20°C is included in **Table 19**.

Table 19. Rate constant (1/week) for Reaction 2, fit to A = PBNA and B = PBNA-NO.

T (°C)	Fit range (weeks)	k(PBNA)	k(PBNA-NO)	$k_{ave}(2)$
20	predicted	N/A	N/A	0.00075
35	[0, 21]	0.01276	0.01258	0.01267
45	[0, 21]	0.04618	0.04187	0.04425
55	[0, 6]	0.13583	0.11933	0.12758

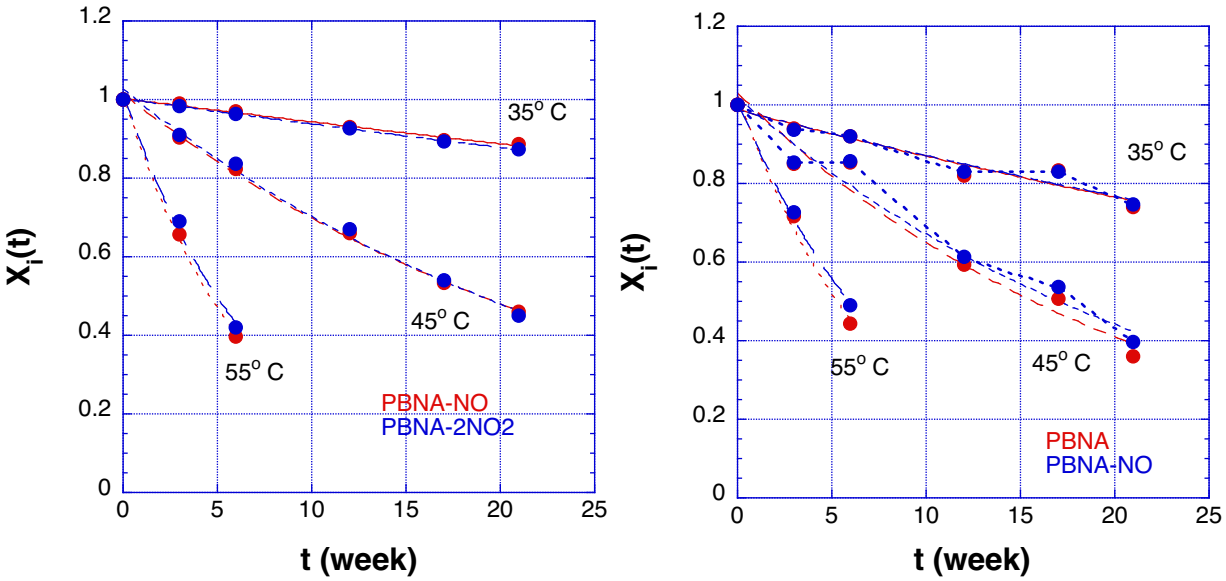

Figure 23. Reaction progress $X_i(t)$ for Reaction 1: i = PBNA-NO (red dots); i = PBNA-$2NO_2$ (blue dots). Lines are exponential fits to the data of C samples (left). Reaction progress $X_i(t)$ for Reaction 2: i = PBNA (red dots); i = PBNA-NO (blue dots). Lines are exponential fits to the data of P samples (right).

From the Arrhenius fits, the energy of activation E_a = 97 and 134 kJ/mol, respectively, for Reaction 1 (PBNA-NO → PBNA-$2NO_2$) and Reaction 2 (PBNA → PBNA-NO). Reaction 1 is slower than Reaction 2 at 35°C and 45°C, but is faster at 55°C. Using the Reaction 2 rate constant predicted for T = 20°C (typical storage conditions), we predict that 15.6 wt.% of the PBNA remains after 51 years (reduced from 6339 µM to 990 µM). This compares quite well with the qualification test measurement for the 51-year-old baseline NP, where [PBNA] = 757 µM. Based on this result, nitrosation from PBNA to PBNA-NO is likely the dominant reaction mechanism for the NP in storage.

4. Conclusion

In this ANTA experiment, a total of 158 samples of 8 different treatments were aged at four moderate temperatures to study the isolated interactions between PBNA, HNO_3, and NP. The detection of m/z 249.1027 and the identification of PBNA-NO finally resolve the mystery of insource fragment m/z 219.1047. The mechanism of PBNA degradation is thoroughly explained if not fully uncovered. The identification of PBNA-NO further provides additional solid evidence for supporting HONO elimination as a key degradation mechanism in the early stage of NP aging. Based on the kinetic analysis of two key reactions, PBNA to PBNA-NO and PBNA-NO to PBNA-$2NO_2$, high accuracy is achieved in our prediction of PBNA consumption, which also explains the earliest event of NP degradation in correlation with PBNA and how much our NPs have been aged naturally. Additionally, the ANTA experiment has proven that PBNA can scavenge both HONO and HNO_3 through their breakdown products of $NO_2^{\bullet}$, NO_2^+, and NO^+, which reduces the acidity in NP materials. Further studies will be continued on the elucidation of other m/z species found in

NP degradation process and the compilation of all details discovered in the 44-month aging experiment. Furthermore, a library of degraded NP fragments can be constructed to aid in the long-term storage and use of NP.

Acknowledgments

We thank Paul Peterson for fruitful discussion of NP degradation, Phil Leonard for the discussion of the intramolecular rearrangement of NO_x groups in PBNA molecule. This work was supported by the US Department of Energy through the Los Alamos National Laboratory Aging and Lifetimes Program. Los Alamos National Laboratory is operated by Triad National Security, LLC, for the National Nuclear Security Administration of U.S. Department of Energy (Contract No. 89233218CNA000001).

Reference:

[1] C. H. Wong, A. S. Edgar, D. Yang, Liquid Chromatography Mass Spectrometry Study of a Eutectic Mixture of bis(2,2-Dinitropropyl) Acetal/Formal. *Propellants Explos. Pyrotech.* **2021,** *46* (12), 1849-1859.
[2] D. Yang, A. S. Edgar, J. A. Torres, J. C. Adams, J. D. Kress, Thermal Stability of a Eutectic Mixture of Bis(2,2-dinitropropyl) Acetal and Formal: Part C. Kinetic Compensation Effect. *Propellants Explos. Pyrotech.* **2020,** *46* (1), 134-149.
[3] D. Yang, R. Pacheco, S. Edwards, J. Torres, K. Henderson, M. Sykora, P. Stark, S. Larson, Thermal stability of a eutectic mixture of bis(2,2-dinitropropyl) acetal and formal: Part B. Degradation mechanisms under water and high humidity environments. *Polym. Degrad. Stab.* **2016,** *130*, 338-347.
[4] D. Yang, R. Pacheco, S. Edwards, K. Henderson, R. Wu, A. Labouriau, P. Stark, Thermal stability of a eutectic mixture of bis(2,2-dinitropropyl) acetal and formal: Part A. Degradation mechanisms in air and under nitrogen atmosphere. *Polym. Degrad. Stab.* **2016,** *129*, 380-398.
[5] D. Yang, D. Z. Zhang, Role of water in degradation of nitroplasticizer. *Polym. Degrad. Stab.* **2019,** *170*.
[6] K. Chen, A. S. Edgar, J. Jung, J. D. Kress, C. H. Wong, D. Yang, Liquid Chromatography Quadrupole Time-of-Flight Mass Spectrometry Analysis of Eutectic Bis(2,2-dinitropropyl) Acetal/Formal Degradation Profile: Nontargeted Identification of Antioxidant Derivatives. *ACS Omega* **2022,** *7* (39), 35316-35325.
[7] K. Chen, A. S. Edgar, Z. Li, O. C. Marina, D. Yang, Roles of HNO_x and Carboxylic Acids in Thermal Stability of Nitroplasticizers. *ACS Omega* **2023,** *8*, 14730-14741.
[8] G. D. Robertson, Jr., D. M. Mason, W. H. Corcoran, The Kinetics of the Thermal Decomposition of Nitric Acid in the Liquid Phase. *The Journal of Physical Chemistry* **1955,** *59* (8), 683-690.
[9] S. A. Stern, J. T. Mullhaupt, W. B. Kay, The Physicochemical Properties of Pure Nitric Acid. *Chemical Reviews* **1960,** *60* (2), 185-207.
[10] Y. Ziouane, G. Leturcq, New Modeling of Nitric Acid Dissociation Function of Acidity and Temperature. *ACS Omega* **2018,** *3* (6), 6566-6576.
[11] J. Chlistunoff, K. J. Ziegler, L. Lasdon, K. P. Johnston, Nitric/Nitrous Acid Equilibria in Supercritical Water. *J. Phys. Chem. A* **1999,** *103* (11), 1678-1688.
[12] L. Wingen, A. L. Sumner, D. Syomin, K. Ramazan, B. Finlayson-Pitts, Hetergeneous Formation of Nitrous Acid in Laboratory Systems. **2003**.

[13] T. C. Brüggemann, M.-D. Przybylski, S. P. Balaji, F. J. Keil, Theoretical Investigation of the Mechanism of the Selective Catalytic Reduction of Nitrogen Dioxide with Ammonia on H-Form Zeolites and the Role of Nitric and Nitrous Acids as Intermediates. *The Journal of Physical Chemistry C* **2010,** *114* (14), 6567-6587.
[14] D. Yang, J. A. Torres, K. C. Henderson, K. J. Cluff, J. C. Adams, A. S. Edgar, Stability of Naturally Aged Nitroplasticizer. LA-UR-18-23141. Los Alamos National Laboratory, Los Alamos, NM 87545, **2018**.
[15] K. Chen, A. S. Edgar, C. H. Wong, D. Yang, Liquid Chromatography Quadrupole Time-of-Flight Mass Spectrometry: A Strategy for Optimization, Characterization, and Quantification of Antioxidant Nitro Derivatives. *ACS Omega* **2022,** *7* (36), 32701-32707.
[16] A. S. Edgar, C. H. Wong, K. Chen, D. A. Langlois, D. Yang, Identification of 2,2-dinitropropanol, a Hydrolyzed Product of Aged Eutectic Bis(2,2-dinitropropyl) Acetal – Bis(2,2-dinitropropyl) Formal Mixture. *Propellants Explos. Pyrotech.* **2022**.
[17] J. D. Pfaff, U.S. Environmental Protection Agency, EPA Method 300.0: Determination of Inorganic Anions by Ion Chromatography. Revision 2.1. **1993**.
[18] M. Balcerzak, D. Kapica, Fast Ion Chromatographic Method for the Determination of Formates in Alcoholic Drinks. *Food Analytical Methods* **2017,** *10* (7), 2358-2364.
[19] E. Defossez, J. Bourquin, S. von Reuss, S. Rasmann, G. Glauser, Eight key rules for successful data-dependent acquisition in mass spectrometry-based metabolomics. *Mass Spectrom Rev* **2023,** *42* (1), 131-143.
[20] T. Kind, H. Tsugawa, T. Cajka, Y. Ma, Z. Lai, S. S. Mehta, G. Wohlgemuth, D. K. Barupal, M. R. Showalter, M. Arita, O. Fiehn, Identification of small molecules using accurate mass MS/MS search. *Mass Spectrom Rev* **2018,** *37* (4), 513-532.
[21] J. D. Whitman, K. L. Lynch, Optimization and Comparison of Information-Dependent Acquisition (IDA) to Sequential Window Acquisition of All Theoretical Fragment Ion Spectra (SWATH) for High-Resolution Mass Spectrometry in Clinical Toxicology. *Clin Chem* **2019,** *65* (7), 862-870.
[22] G. L. Andrews, B. L. Simons, J. B. Young, A. M. Hawkridge, D. C. Muddiman, Performance characteristics of a new hybrid quadrupole time-of-flight tandem mass spectrometer (TripleTOF 5600). *Anal. Chem.* **2011,** *83* (13), 5442-6.
[23] T. K. Koo, M. Y. Li, A Guideline of Selecting and Reporting Intraclass Correlation Coefficients for Reliability Research. *J Chiropr Med* **2016,** *15* (2), 155-63.
[24] P. Y. Bruice, Chapter 15.11 - the mechanism for the reaction of amines with nitrous acid. In *Organic Chemistry*, 5th ed.; Pearson Prentice Hall: Upper Saddle River, NJ, **2007**; pp 704-706.
[25] D. L. H. Williams, The mechanism of the Fischer-Hepp rearrangement of aromatic N-nitroso-amines. *Tetrahedron* **1975,** *31* (10), 1343-1349.
[26] J. C. Beard, T. M. Swager, An Organic Chemist's Guide to N-Nitrosamines: Their Structure, Reactivity, and Role as Contaminants. *J Org Chem* **2021,** *86* (3), 2037-2057.
[27] S. González-Mancebo, E. Calle, M. P. García-Santos, J. Casado, Inhibition of Nitrosation by Steric Hindrance. *Journal of Agricultural and Food Chemistry* **1997,** *45* (2), 334-336.
[28] Y. Ogata, H. Tezuka, Kinetics of the nitric acid oxidation of nitrosophenol to nitrophenol. *The Journal of Organic Chemistry* **1968,** *33* (8), 3179-3181.